

**IZMIR KATIP CELEBI UNIVERSITY ★ GRADUATE SCHOOL OF SCIENCE AND
ENGINEERING**

**INCREASING THE EFFICIENCY OF ORGANIC LIGHT EMITTING DIODE
BY USING SELF ASSEMBLED MONOLAYER**



M.Sc. THESIS

Eyyup YALÇIN

Department of Materials Science and Engineering

Thesis Advisor: Assoc. Prof. Dr. Mustafa CAN

February 2016

**IZMIR KATIP CELEBI UNIVERSITY ★ GRADUATE SCHOOL OF SCIENCE AND
ENGINEERING**

**INCREASING THE EFFICIENCY OF ORGANIC LIGHT EMITTING DIODE
BY USING SELF ASSEMBLED MONOLAYER**

M.Sc. THESIS

**Eyyup YALÇIN
(Y130111024)**

Department of Materials Science and Engineering

Thesis Advisor: Assoc. Prof. Dr. Mustafa CAN

February 2016

İZMİR KÂTİP ÇELEBİ ÜNİVERSİTESİ ★ FEN BİLİMLERİ ENSTİTÜSÜ

**KENDİLİĞİNDEN ORGANİZE TEK KATMAN TABAKALARI
KULLANILARAK ORGANİK IŞIK YAYAN DİYOTLARIN VERİMİNİN
ARTIRILMASI**

YÜKSEK LİSANS TEZİ

**Eyyup YALÇIN
(Y130111024)**

Malzeme Bilimi ve Mühendisliği Ana Bilim Dalı

Tez Danışmanı: Doç. Dr. Mustafa CAN

ŞUBAT 2016

Eyyup YALÇIN, a **M.Sc.** student of **IKCU Graduate School of Science and Engineering**, successfully defended the thesis entitled **”INCREASING THE EFFICIENCY OF ORGANIC LIGHT EMITTING DIODE BY USING SELF ASSEMBLED MONOLAYER”**, which he prepared after fulfilling the requirements specified in the associated legislations, before the jury whose signatures are below.

Thesis Advisor : **Assoc. Prof. Dr. Mustafa CAN**
Izmir Katip Çelebi University

Jury Members : **Assoc. Prof. Dr. Şerafettin DEMİÇ**
Izmir Katip Çelebi University

Assist. Prof. Dr. Hadi M. ZAREIE
Izmir Institute of Technology

Date of Submission : 15.02.2016

Date of Defense : 24.02.2016



To my family,

ACKNOWLEDGMENTS

Many people deserve a thank you for their support during my M.Sc. program and I have already apologized to whomever I am forgetting in the following list. Firstly and foremost, I would like to thank my advisor, Assoc. Prof. Dr. Mustafa CAN, for his leading and support during my master thesis. Then I have to thank Assoc. Prof. Dr. Şerafettin Demić for his open-minded ideas in this study. Moreover, my fellow lab mates M. Zeliha Yiğit and Emre Arkan deserve my special thanks for supporting me in chemical issue by providing new synthesized materials.

I would like to thank Assoc. Prof. Dr. Mahmut KUŞ who gave me a chance to access the laboratory and research facilities in Selçuk University Advanced Technology Research and Application Centre. I also wish to express my gratitude for Koray Kara and Duygu Akın Kara. It would have been impossible to achieve these research results without their help and experience. In addition, I want to thank my dear friend Veysel Ulaş for his help to organize this thesis.

Last but not least, I would like to thank my family. I cannot find words to express my thanks for their helps.

TABLE OF CONTENTS

	<u>Page</u>
ACKNOWLEDGMENTS	vii
TABLE OF CONTENTS	viii
ABBREVIATIONS	ix
LIST OF TABLES	x
LIST OF FIGURES	xi
ABSTRACT	xii
ÖZET	xiii
1. INTRODUCTION	1
1.1 Organic Light Emitting Diodes	1
1.2 Device Structure of OLEDs	4
1.3 Charge Injection	5
1.4 Materials	7
1.4.1 Anode materials	7
1.4.2 Hole transport materials (HTL)	7
1.4.3 Electron transport and emissive materials (ETL and EM)	8
1.4.4 Cathode materials	9
1.5 Self-Assembled Monolayers	9
1.6 OLED Efficiency	11
2. EXPERIMENTAL DETAILS	13
2.1 The Steps of OLED Preparation	13
2.2 Etching, Cleaning and Oxygen Plasma procedure for ITO	13
2.3 Surface Treatment of ITO by Using SAM Technique	14
2.4 Thermal Evaporation of Organic Layers and Metallic Layer	15
2.5 Characterization of OLED Devices	17
2.5.1 AFM surface characterization	18
2.5.2 Kelvin probe force microscopy (KPFM) surface characterization	19
2.5.3 Cyclic voltammetry characterization	20
2.5.4 Contact angle characterization	20
3. RESULT AND DISCUSSION	22
3.1 Electrical and Optical Characterization Results	22
3.1.1 Cycle voltammetry results	22
3.1.2 Electrical and optical characterization of 4,4"-di-9H-carbazol-9-yl- 1,1':3',1"-terphenyl-5'-carboxylic acid (CAR)	24
3.1.3 Electrical and optical characterization of 4,4"-bis(diphenylamino)- 1,1':3',1"-terphenyl-5'-carboxylic acid (TPA)	29
3.1.4 Electrical and optical characterization of 'TPA and CAR' materials	33
3.2 Surface Characterization Results	38
3.2.1 Atomic force microscope results	38
3.2.2 Kelvin probe force microscope results	39
3.2.3 Contact angle results	42
4. CONCLUSIONS	43
REFERENCES	46

ABBREVIATIONS AND SYMBOLS

a.u	: Absorption unit
AFM	: Atomic Force Microscope
Ag	: Silver
Al	: Aluminum
Au	: Gold
Ca	: Calcium
cd	: candela
EL	: Electroluminescence
EML	: Emissive Layer
EQE	: External Quantum Efficiency
ETL	: Electron Transport Layer
ev	: Electron Volt
HOMO	: Highest Occupied Molecular Orbital
HTL	: Hole Transport Layer
HTM	: Hole Transport Material
IQE	: Internal Quantum Efficiency
ITO	: Indium Tin Oxide
J	: Current Density
KPFM	: Kelvin Probe Force Microscope
L	: Luminance
LCD	: Liquid Crystal Diode
Li	: Lithium
lm	: lumen
LUMO	: Lowest Unoccupied Molecular Orbital
M	: Molar
Mg	: Magnesium
MoO₃	: Molybdenum trioxide
N	: Nitrogen
η_{ce}	: Current Efficiency
η_{ext}	: External Quantum Efficiency
η_{int}	: Internal Quantum Efficiency
η_p	: Power Efficiency
OLED	: Organic Light Emitting Diode
RMS	: Root mean square
SAM	: self Assemble Monolayer
T_g	: Glass Transition Temperature
V_{CPD}	: Contact potential difference
W	: watt
γ_{lv}	: liquid-vapor surface tension
γ_{sl}	: solid- liquid surface tension
γ_{sv}	: solid-vapor surface tension
θ	: Young contact angle

LIST OF TABLES

	<u>Page</u>
Table 2.1 : Configuration of OLED devices	17
Table 3.1 : Device numbers and their structures	25
Table 3.2 : Electrical and Optical details about devices	29
Table 3.3 : Device structures and theirs numbers	30
Table 3.4 : Electrical and Optical details about devices.	33
Table 3.5 : Device numbers and structures	34
Table 3.6 : Electrical and Optical details about devices	37
Table 3.7 : Surface roughness of Bare ITO, ITO/CAR, ITO/TPA and ITO/TPD/Alq3	38
Table 3.8 : Surface potential of Bare ITO and modified ITO with CAR and TPA...	42



LIST OF FIGURES

	<u>Page</u>
Figure 1.1 : LG OLED display (a) and OLED for lighting applications (b) [6]	3
Figure 1.2 : OLED materials can be deposited on flexible substrate	3
Figure 1.3 : General Structure of an OLED	4
Figure 1.4 : Hole and electron injection from electrodes to organic layers.	6
Figure 1.5 : OLED structure with the hole and electron blocking layers.	6
Figure 1.6 : Chemical Structure of TPD (a) and NPB (b).....	7
Figure 1.7 : Chemical Structures of Alq ₃ (a), Gaq ₃ (b) and Inq ₃ (c).....	8
Figure 1.8 : Schematic illustration of SAMs (a) – Generation of SAMs on a substrate (b) 10	10
Figure 1.9 : Surface coverage of SAM versus time	11
Figure 2.1 : Manufacturing process of OLEDs	13
Figure 2.2 : Oxygen Plasma Device	14
Figure 2.3 : Chemical structure of TPA (a) and CAR (b) Molecules	15
Figure 2.4 : Organic (a) and Metallic (b) Evaporation Systems	16
Figure 2.5 : General work principle of AFM	18
Figure 2.6 : Nanosurf Flex AFM (right) and its software (left)	19
Figure 2.7 : Typical current vs potential graph of CV	20
Figure 2.8 : Illustration of contact angles on a smooth solid surface	21
Figure 3.1 : CV Voltammogram of modified ITO with TPA	23
Figure 3.2 : CV Voltammogram of modified ITO with CAR.....	23
Figure 3.3 : Energy diagram of OLED devices with TPA (a) and CAR (b).....	24
Figure 3.4 : J-V Characteristic of Device 1 to 4.....	25
Figure 3.5 : Luminance versus Voltage graph of Device 1 to 4.....	26
Figure 3.6 : Current Efficiency vs Luminance graph of Device 1 to 4.....	27
Figure 3.7 : Power Efficiency vs Luminance graph of Device 1 to 4	28
Figure 3.8 : Intensity vs Wavelength graph for Device 1 to 4	29
Figure 3.9 : Current Density versus Voltage graph	30
Figure 3.10 : Luminance versus Voltage graph.....	31
Figure 3.11 : Current Efficiency versus Luminance graph.....	32
Figure 3.12 : Power Efficiency versus Luminance graph.....	32
Figure 3.13 : Intensity versus Wavelength Graph	33
Figure 3.14 : Current Density versus Voltage graph	35
Figure 3.15 : Luminance versus Voltage graph.....	35
Figure 3.16 : Current Efficiency versus Luminance graph.....	36
Figure 3.17 : Power Efficiency versus Luminance graph.....	36
Figure 3.18 : Intensity versus Wavelength graph.....	37
Figure 3.19 : AFM images of Bare ITO (a), modified ITO with CAR (b) and TPA (c). After organic materials coating on ITO (d).....	38
Figure 3.20 : AFM topography (a) and surface potential (b) of bare ITO with KPFM.	39
Figure 3.21 : AFM topography (a) and surface potential (b) of ITO/CAR with KPFM technique	39
Figure 3.22 : AFM topography (a) and surface potential (b) of ITO/TPA with KPFM	40
Figure 3.23 : Surface Potential of Bare ITO	41
Figure 3.24 : Surface Potential of ITO/CAR.....	42
Figure 3.25 : Surface Potential of Bare ITO, ITO/CAR and ITO/TPA	41
Figure 3.26 : Contact angle on Bare ITO (a), ITO/CAR (b) and ITO/TPA (c)	42
Figure 4.1 : Photos of OLED devices	45

INCREASE EFFICIENCY OF ORGANIC LIGHT EMITTING DIODE BY USING SELF-ASSEMBLED MONOLAYERS

ABSTRACT

This study is focused on modification and characterization of indium tin oxide (ITO) substrates with self-assembled monolayers (SAMs) to increase efficiency of Organic Light Emitting Diodes (OLEDs). As known, ITO has widely been used as an anode material in OLED devices because of its high conductivity and high transparency. However the work function between the energy level of ITO electrode and HOMO energy level of organic materials have a large injection barrier. This barrier leads poor charge injection and low efficiency. To solve this problem ITO substrates are modified using SAM materials, hence the energy level of ITO is increased.

In this thesis, 4,4''-bis(diphenylamino)-1,1':3',1''-terphenyl-5'-carboxylic acid (TPA) and 4,4''-di-9*H*-carbazol-9-yl-1,1':3',1''-terphenyl-5'-carboxylic acid (CAR) molecules were used as SAM materials. After ITO substrates were modified with SAM materials, changing in an energy level of ITO was determined using Cyclic Voltammetry. In addition, the OLED devices which are fabricated with SAM modified ITO show better turn on voltage, luminance, current efficiency, power efficiency and intensity compared to unmodified ITO.

For the surface characterization, Atomic Force Microscope (AFM) was used to analyze surface topography of the modified and unmodified ITO. Also, Kelvin Probe Force Microscope (KPFM) was used to determine changes in the surface potential of modified and unmodified ITO. Finally, surface characterization was analyzed with contact angle measurement. After ITO was modified with CAR and TPA molecules, contact angle variation between modified and unmodified ITO was clearly observed.

**KENDİLİĞİNDEN ORGANİZE TEK KATMAN TABAKALARI
KULLANILARAK ORGANİK IŞIK YAYAN DİYOTLARIN VERİMİNİN
ARTIRILMASI**

ÖZET

Bu çalışma, organik ışık yayan diyotların (OLEDs) verimini artırmak için indiyum kalay oksit (ITO) yüzeyinin kendiliğinden organize tek katman tabakaları (SAM) ile modifiye ve karakterizasyonu üzerine yoğunlaşmıştır. Bilindiği gibi, ITO yüksek iletkenlik ve yüksek saydamlık özelliğinden dolayı OLED cihazlarında yaygın olarak anot malzemesi olarak kullanılmaktadır. Fakat metal elektrotun (ITO) çalışma fonksiyonu ile organik malzemelerin HOMO enerji seviyesi arasında yüksek enjeksiyon farkı bulunmaktadır. Bu fark, düşük yük enjeksiyonuna ve düşük verime neden olmaktadır. Bu problemi çözmek için ITO yüzeyleri SAM malzemeleri ile modifiye edilmiştir. Böylelikle ITO nun enerji seviyesi yükseltilmiştir.

Bu tezde SAM malzemeleri olarak 4,4"-bis(difenilamino)-1,1':3,1"-terfenil-5'-karboksilik asit (TPA) ve 4,4"-di-9*H*-karbazol-9-il-1,1':3,1"-terfenil-5'-karboksilik asit (CAR) molekülleri kullanılmıştır. ITO yüzeyleri SAM malzemeleri ile modifiye edildikten sonra, ITO nun enerji seviyesindeki değişim döngüsel voltametri ile belirlenmiştir. Ayrıca, SAM ile modifiye edilmiş ITO yüzeylerinden üretilen OLED cihazları, modifiye edilmemiş ITO yüzeylerinden elde edilen OLED cihazlarına göre daha iyi çalışma gerilimine, parlaklığa, akım verimine, güç verimine ve ışık yoğunluğuna sahiptirler.

Yüzey karakterizasyonu için, modifiye edilmiş ve modifiye edilmemiş ITO yüzeyinin topografyası Atomik Kuvvet Mikroskobu (AFM) kullanılarak analiz edilmiştir. Ayrıca modifiye edilmiş ve modifiye edilmemiş ITO yüzeyindeki potansiyel değişimi Kelvin Prope Kuvvet Mikroskobu (KPFM) ile analiz edilmiştir. Son olarak yüzey karakterizasyonu temas açısı ile incelenmiştir. ITO 'CAR ve TPA' molekülleri ile modifiye edildikten sonra, modifiye edilmiş ve modifiye edilmemiş ITO lar arasındaki temas açısı değişimi açıkça gözlemlenmiştir..

1. INTRODUCTION

1.1 Organic Light Emitting Diodes

Energy is one of the main problems in the history of mankind. Especially after the industrial revolution, energy needs increased dramatically. By discovery of carbon based fuel sources, almost all countries shifted their preferences to use this type of energy source. However, excessive use of fuel energy sources causes tragic problems to mankind such as air pollution, which is one of the biggest treats for a human being, recently. Because of this problem, researchers are actively searching the ways for converting green energy sources like solar energy, wind energy, etc, into electrical energy.

There have been many technological applications applied to our life in the past 60 years, which made a big increment in mechanization of human kind. As known, almost every technical equipment consumes energy to produce effective work. Relatedly, a huge amount of fuel source is being used up giving rise to the air pollution. For this reason, researchers densely study on developing energy saving materials for a long time that will decline air pollution. The materials that are used in organic light emitting diodes (OLEDs) are one of these novel materials and scientists have researched by scientists since the discovery of electroluminescence.

The first electroluminescence (EL) property of organic materials in OLEDs was shown by Helfrich and Schneider in 1965 [1]. Nevertheless, it had extremely high turn on voltage (~100V) for which almost no practical application seemed possible for those times. Fortunately, after 22 years later in 1987 the first efficient low-voltage (10V) organic EL was demonstrated by Tang and VanSlyke [2] in Kodak. It is considered as the beginning of the first OLEDs. They fabricated this device with thermal evaporation technique under high vacuum by using small organic molecules. These molecules include N,N-diphenyl-N,N-bis (3-methylphenyl) 1-1' biphenyl – 4,4 diamine (TPD) and tris (8-hydroxyquinoline) aluminum (Alq_3) with a total thickness of about 100 nm in a double layer structure. The study on organic electronic devices

increased in huge amounts after this invention, which is regarded a milestone in this field. With this development, OLEDs have attracted much attention and taken a part in the market as displays. Another important development about OLEDs occurred in 1990 at the University of Cambridge. In this development researchers obtain electroluminescence from polymers[3]. They used a conjugated polymer, poly-para-phenylene vinylene (PPV)[4], which become the most used polymers in OLEDs. This discovery opens the gate for flexible electronics.

Today OLEDs are used as displays and lighting appliance (Figure 1.1) due to their advantage of low-power consumption, high contrast, high brightness, low weight, high luminous efficiency and wide viewing angle [5]. Due to that they are widely used their electric energy consumption should be lowered. Hence, low power consumption is the most important property for OLEDs. These above listed properties of OLEDs make it advantageous compared to liquid crystal displays (LCDs) in the market. Because, LCD displays use polarized films since the light requires to be polarized. In addition, color filters should also be used in LCDs, because LCDs cannot emit different colors directly like OLEDs. There is an instant light loss of 50% due to the problem of polarized films and color filters. In addition, in OLED displays only active pixels are turned on and inactive pixels do not need any power. Nevertheless, LCD displays need the same power for their backlight as well. Hence, the backlight is lit all the time whether a black or a white picture is displayed[3]. Due to this property, we can say that a large amount of energy will be saved if they are widely used in TV screens, computer screens, mobile phone screens, MP3 player, car radios, digital cameras etc. and especially in lighting applications. Consequently, it makes OLEDs very important for now and future technologies.



(a)



(b)

Figure 1.1 : LG OLED display (a) and OLED for lighting applications (b) [6]

A new trend in OLEDs is deposition of their materials on flexible plastics (Figure 1.2). This brings many advantages like eliminating the fragile and heavy glass substrate. In this process, OLED materials are fabricated on flexible substrate by generally using a spin coating technique which is a relatively cheap coating method.



Figure 1.2 : OLED materials can be deposited on flexible substrate (URL1)

Beside all of the advantages as explained above, OLEDs have some disadvantages like low lifetime, instability of organic components, expensive manufacturing

process and also it can be damaged easily when exposed to water. These problems are still unsolved and need investigation by researchers.

1.2 Device Structure of OLEDs

The general structure of OLEDs was shown in Figure 1.3. It consists of a light emissive layer (EL), a hole transport layer (HTL) and an electron transport layer (ETL). These layers are sandwiched between two metal electrodes. One of these electrodes should be transparent so that light can be perceived.

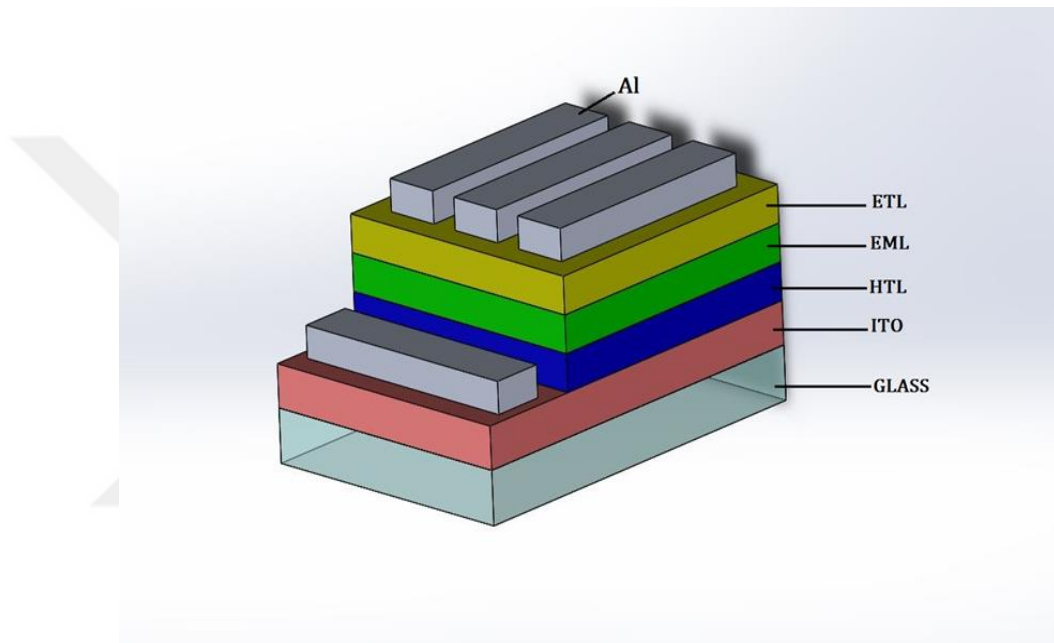


Figure 1.3 : General Structure of an OLED

Beside these layers, hole injection layers can be used between indium tin oxide and organic layers to help reduce the energy barriers at the electrode-organic interface and facilitate the transportation of the charge carriers [7]. The orbital energy of the electrodes should match the energy of used organic material as much as possible, in order for them to be used as anode/cathode layers. Indium tin oxide is usually used as an anode electrode because its work function is close to the highest occupied molecular orbital (HOMO) energies of the organic materials acting as an HTL. In addition, Ca, Al and Mg are generally preferred as cathode electrodes because of their low work function [8].

The total thickness of an OLED is generally less than 350 nm. Such scale of thickness provides transparency to OLEDs. So that light absorption of organic materials can be minimized.

OLEDs are usually fabricated on rigid glass substrates and flexible polymer substrates. These substrates are coated with a transparent conductive layer and it is usually used as the anode electrode. If a flexible substrate is used, the low thickness of the organic layer ensures OLEDs flexibility.

1.3 Charge Injection

The selection of OLED materials has an important role in efficiency. Hence, charge injection and charge transport of the materials should be increased to realize charge balance in order to achieve high efficiency in OLED devices. In addition, the energy level of organic materials and electrodes should be selected as closely as possible for this aim. Because the charge balance of the electrode-organic layer interface has an important role [9].

There are various techniques to improve the charge injection. Most of these techniques have been reported on modification of ITO such as oxygen plasma, ultraviolet ozone, self-assemble monolayers (SAMs), ultra-thin layer such as MoO_3 and graphene oxide [10].

The work principle of an OLED is illustrated in Figure 1.4. If voltage is applied between two electrodes, holes start moving from anode to the organic layer where electrons start moving from the cathode to the organic layer. The mobility of holes and electrons moving inside organic materials has generally come in existence by hopping processes. After diffusion of electrons and holes, a recombination is occurred which produces excitons, meantime photons are emitted [3].

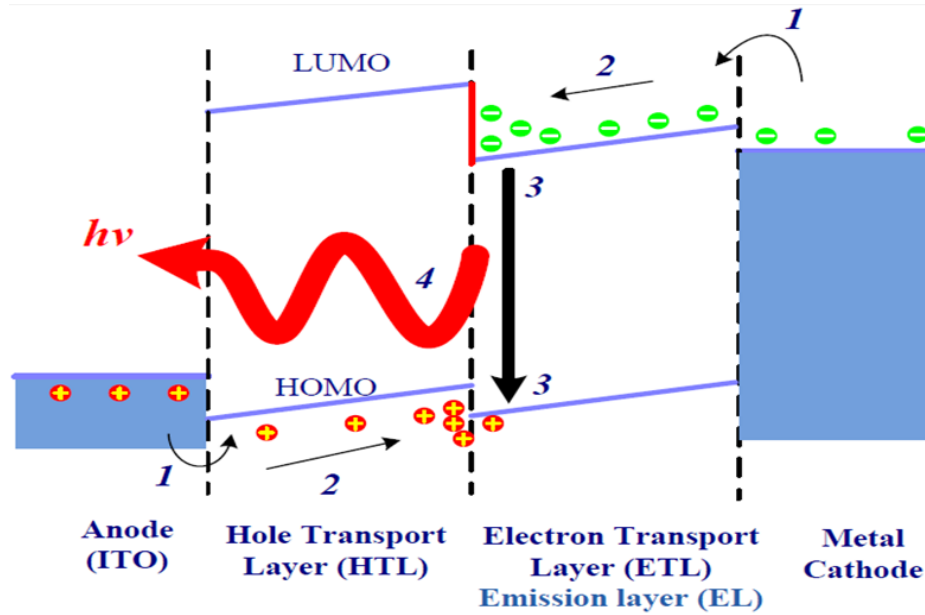


Figure 1.4 : Hole and electron injection from electrodes to organic layers.

The interface between HTL and EL acts as an electron blocking barrier. Similarly, the interface between ETL and EL acts as a hole blocking barrier. If HTL and ETL were not used as electron and hole blocking barriers, OLEDs structure would become more complex. In that case the OLED would be consisting of two additional layers similar to that is shown in Figure 1.5 [11].

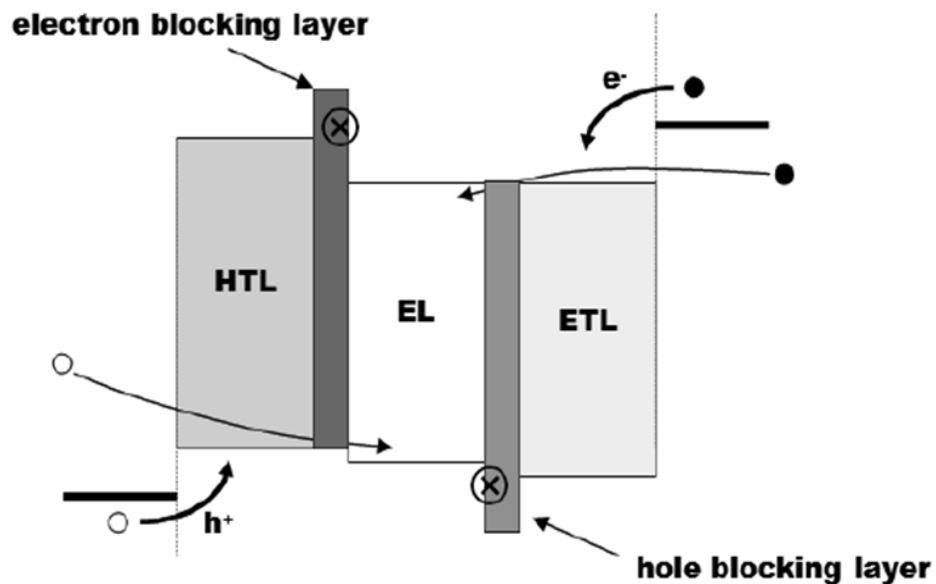


Figure 1.5 : OLED structure with the hole and electron blocking layers [11].

1.4 Materials

1.4.1 Anode materials

Indium tin oxide is one of the most widely used anode materials in OLED devices because of its high electrical conductivity ($\sim 2 \times 10^{-4} \Omega\text{cm}$), low work function (~ 4.8 eV) and high transparency ($\sim 90\%$ at 550nm) in the visible range [12, 13]. Also the work function of ITO is very close to the HOMO energy level of HTL. This closeness helps OLED to increase hole transport from ITO to HTL materials.

The price of ITO substrates is proportional to indium price [14]. To date, researchers have been studied on many alternative materials replace to ITO since there is a big gap between the price of indium and other abundant materials. However, the materials alternative to ITO have a high work function (5.2-6.1 eV). Hence the hole injection efficiency is decreased and OLED performance degraded [15]. Because of these problems, ITO is still the best alternative anode material for OLED devices compared to others.

1.4.2 Hole transport materials (HTL)

Hole Transport Materials have an important role in OLEDs device performance. Generally, triarylamine compounds have been used as hole-transport materials since the first fabrication of OLEDs in 1987. In lots of various triarylamine compounds N, N'-diphenyl-N, N'-bis(3-methylphenyl)-(1,1'-biphenyl)-4,4'-diamine (TPD) and N, N'-bis(1-naphthalenyl) – N, N' diphenyl-(1,1'-biphenyl)-4,4'-diamine (NPB) are the most widely used as HTL materials in OLEDs. The chemical structure of these materials are shown in Figure 1.6 [16] [17].

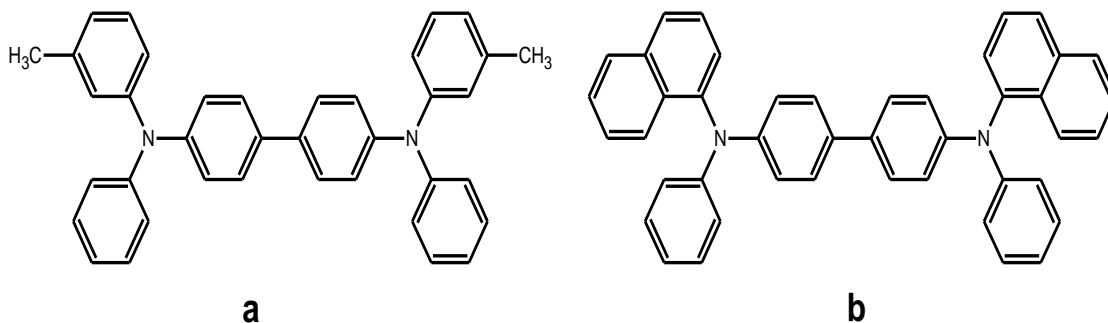


Figure 1.6 : Chemical Structure of TPD (a) and NPB (b)

TPD and NPB are small molecules so that they can easily be evaporated under high vacuum. In addition, this material has lower energy barrier between HOMO energy levels of HTL and the work function of anode. A suitable HTM for electrophosphorence should also has high hole mobility. Since T_g has an important role in high thermal and morphological stability [18] it should also satisfy high glass transition temperature (T_g). The most used hole transport materials, TPD and NPB, have 65 °C and 95 °C T_g , respectively [19].

1.4.3 Electron transport and emissive materials (ETL and EM)

Emissive compounds are the most important materials in OLED devices, because recombination and light emitting occur in emissive layer. Generally, emissive materials (EL) show both electron transport and hole blocking properties.

Mobility of hole transport is about 2 or 3 orders of magnitude higher than electron mobility of electron transport. Hence, EMs should have both high electron mobility and good hole blocking property [20]. Tris-(8-hydroxyquinoline) aluminum (**Alq₃**), tris-(8-hydroxyquinolinolato) gallium (**Gaq₃**) and tris-(8-hydroxyquinoline) indium (**Inq₃**) materials are the most used emissive layer (EM) materials in OLED devices. The chemical structures of these materials are shown in Figure 1.7. Among these materials Alq₃ is the most used ETL and EL because of its good thermal stability, high electron affinity and ionization potential [21].

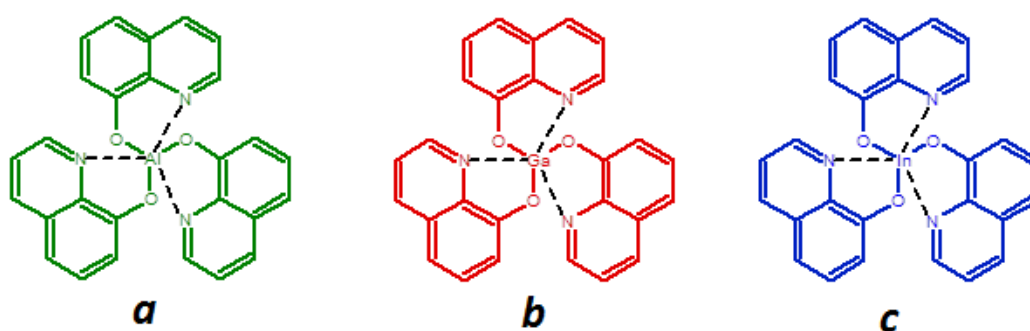


Figure 1.7 : Chemical Structures of Alq₃ (a), Gaq₃ (b) and Inq₃ (c)

A recombination of holes and electrons occur between HTL and ETL. In addition, recombination region can be located in both ETL and HTL. If the recombination region is located in ETL, this layer behaves as the emissive layer (EM). If the recombination region is located in HTL, this layer behaves as emissive layer. Hence,

these devices are structured as successive layers of ITO/HTL/ETL(EM)/Metal or ITO/HTL(EM)/ETL/Metal. Besides, EM can also be coated as a separate layer. In that case, EM is neither in ETL nor in HTL therefore it is sandwiched between HTL and ETL (ITO/HTL/EM/ETL/Metal) [22].

1.4.4 Cathode materials

There must be charge balance between holes and electrons in injection to increase efficiency in OLEDs. As mentioned in previous parts, high barrier between organic layers and metals interface effect holes and electrons injection in a bad manner. In particular, barrier between organic layer and cathode electrode is too large compared to the barrier between organic layer and anode electrode [23, 24].

Unlike anode materials, cathode materials should have low work function. Mg, Ca, Li, Al and Ba are metals that satisfy low work function that are applicable to OLEDs [16]. Among these metals, Al is widely used as cathode material. In addition, LiF buffer layer can be used between Al cathode and organic layer, as well. This buffer layer increase the electron injection, device performance and also provides a longer lifetime [25]

1.5 Self-Assembled Monolayers

In literature, it is reported that indium tin oxide has been modified more than 20 years with several ways. Self-assembled monolayers (SAM) technique is one of the most used modification technique. This method firstly reported by Nuzzo and Allara and they published their study with the title as follows, “Absorption of Biofunctional Organic Disulfides on Gold Surface” in 1983[26]. Hence, Nuzzo and Allara are considered to be the pioneers of the SAMs.

Self-assembled monolayer technique is used to modify indium tin oxide in the literature to enhance hole injection and reduce the turn on voltage, as well [27]. In addition, SAMs have been used to enhance the interfacial compatibility between hydrophilic anode and hydrophobic HTL. Also, SAMs reported in literature as a current blocking layer or a moisture penetration blocking layer for OLEDs[28]. Because, pure adhesion between organic materials and inorganic electrodes is a big problem in OLED devices. This pure adhesion problem limit the performance and degrade the stability of OLED devices [28, 29]. SAM molecules, inherently

smoothly bond with surface and changes the physical and chemical properties of surface although they are very thin layer. The thickness of this layer is about 2 or 3 nanometers. Such small scale makes SAM suitable for organic electronic and nano technological applications. In addition, they are easy to prepare and low cost, hence SAM materials have many applications in technology, such as protective coating, catalysts, biological sensors, optoelectronic devices etc. [30].

The Figure 1.8 SAM materials show the molecular structure of SAMs. As shown, it consists of three main parts; the first part is the surface-active head group, the second part is the spacer groups and the third part is the surface functional groups.

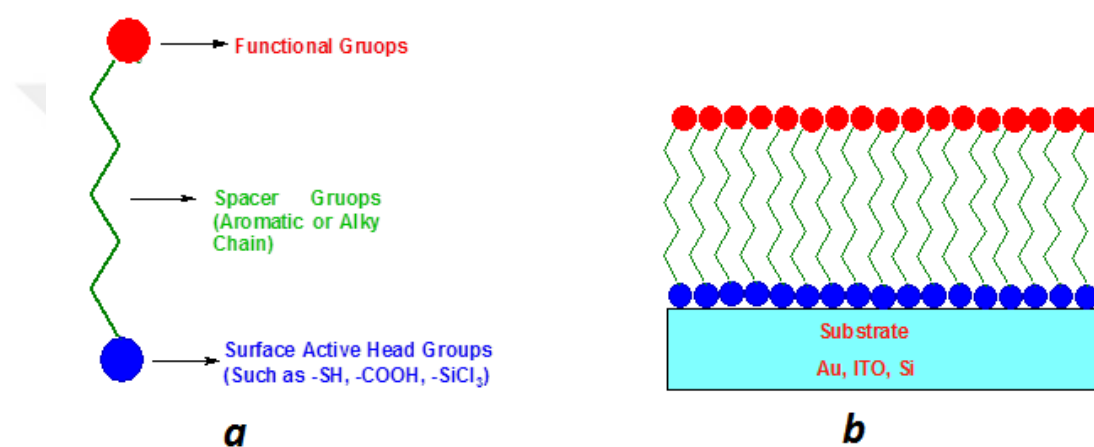


Figure 1.8 : Schematic illustration of SAMs (a) – Generation of SAMs on a substrate
(b)

Surface-active head groups bond with surface spontaneously by strong or weak bonds. Also, surface active head groups provide the physical and chemical interaction on the active device layer. Spacer groups are aromatic or hetero-aromatic in structure. In addition, the spacer group determines the thickness of SAM. The last part, surface functional groups, determines the surface properties of SAMs. Besides, the functional group makes a new bond with the organic layer, such as hole transport layers.

Self-assembled monolayer molecules gradually bond on the surface in a definite period. Figure1.9 shows the increase of the SAM molecule amount with respect to time. As shown, after some time the amount of molecules accumulated on the surface of ITO saturates. Hence, the increase of accumulation by means of keeping ITO inside a SAM solution does not mean it will increase the performance of the manufactured device. Because after a period molecules start to accumulate and this

aggregation effects the device performance in a bad way. The best way to find the suitable time for reaching enough coating thickness is as follows; several ITO is kept inside the SAM solution for different periods of time. Then those several samples are evaluated with respect to their keeping time by means of their electrical device performance. Besides, as shown in the same figure, the coverage of SAM molecules achieves a saturation limit and become stable after a certain time.

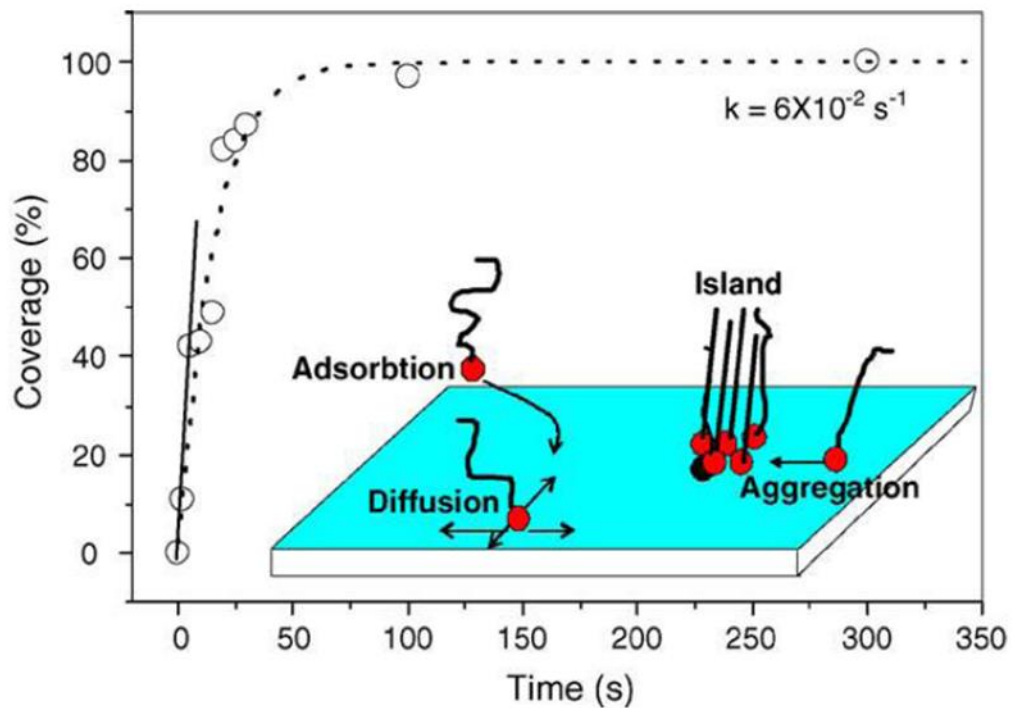


Figure 1.9 : Surface coverage of SAM versus time [31]

1.6 OLED Efficiency

There are a few parameters to determine OLED efficiency. In this part External Quantum Efficiency (EQE), Internal Quantum Efficiency (IQE), current efficiency and power efficiency are explained briefly.

External quantum efficiency (η_{ext}) is the ratio of the number of photons emitted from the surface of an OLED divided by the number of injected electrons. EQE also can be written as the ratio of the total number of photons which is emitted in all direction from the device[32]. The internal quantum efficiency (η_{int}) is the ratio of the total number of photons generated within the organic layer to the number of electrons injected in the device. Hence, EQE and IQE differ by fraction of light

coupled out of structure into viewing direction (η_c) [33]. By this definition, a relationship between EQE and IQE can be written as follows,

$$\eta_{ext} = \eta_{int}\eta_c \quad (1.1)$$

Beside EQE and IQE, current efficiency (cd/A) and power efficiency (lm/W) are most used parameters for determining OLED device performance. For calculation of current and power efficiency of devices, luminance (cd/m^2), voltage (V) and current (I) are used. Current efficiency (η_{ce}) is defined as emitting luminance per unit current[34]. In that case we define η_{ce} as follows,

$$\eta_{ce} = AL/I_{OLED} \quad (2.2)$$

Where L is the luminance of OLED, A is device active area and I_{OLED} is driving current of the device. In addition to the current efficiency, power efficiency (η_p) depend on device voltage, current and luminance, as well. To attain high power efficiency, OLED device should emit high luminance with low current (I) and voltage (V) [35]. Hence η_p is defined as follows,

$$\eta_p = \frac{L}{IV} \quad (2.3)$$

2. EXPERIMENTAL DETAILS

2.1 The Steps of OLED Preparation

The sequential manufacturing process of OLEDs is listed in Figure 2.1.

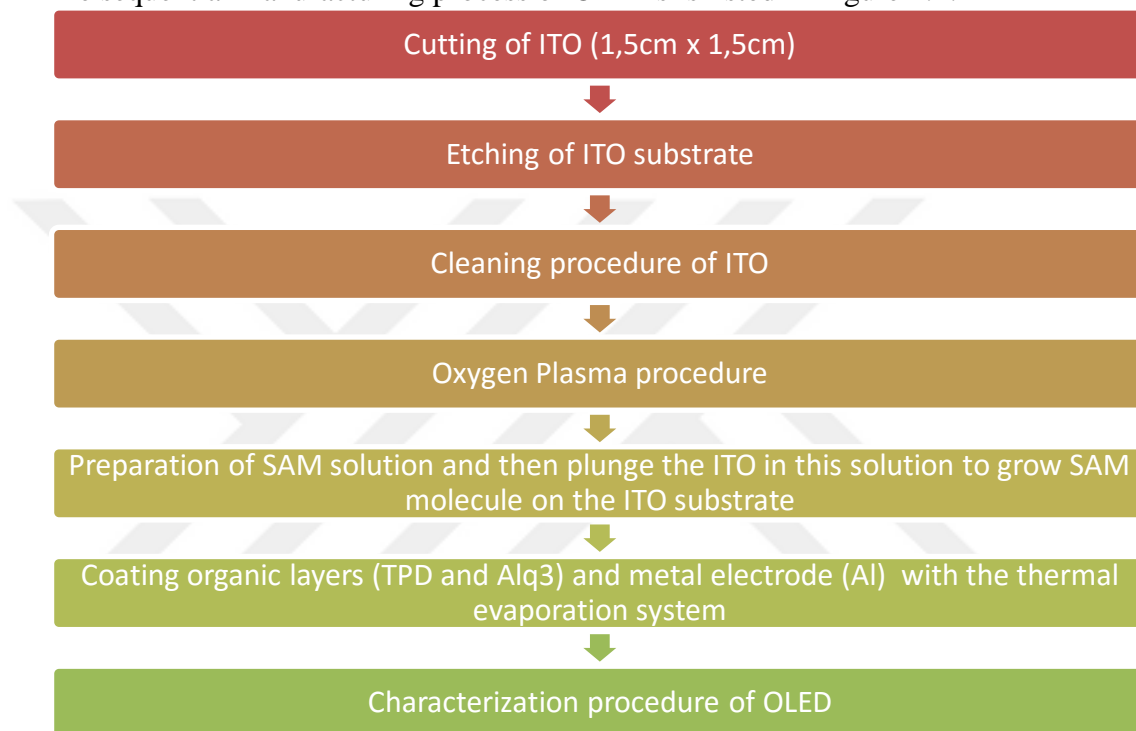


Figure 2.1 : Manufacturing process of OLEDs

2.2 Etching, Cleaning and Oxygen Plasma procedure for ITO

The first step of OLED fabrication was started with cutting the ITO coated glass. The surface resistivity of samples is about 18-24 Ω /sq. First of all ITO glass substrates were cut in a size of 1,5cm x 1,5cm by using a diamond pencil. After cutting process, ITO substrates were etched. Before start to etching, 1,1cm of ITO was covered with tape to prevent this part from the damage during the etching process. And then 0,4 cm ITO was etched by using king water (prepared with 3HCl and 1HNO₃ acids) and this length is defined as cathode. 0,4 cm of ITO substrates were etched to prevent short cut between anode and cathode.

After etching, ITO substrates were cleaned and for this procedure ITO substrates were sonicated in deionized water, acetone and isopropanol respectively for 20 minutes. After cleaning procedure, all of the substrates were dried with nitrogen gas. Then, all of the samples are exposed to oxygen plasma for 8 minutes under vacuum. Oxygen plasma increases the work function of ITO and reduces the barrier for charge injection[36]. As shown in Figure 2.1 electronic diener femto PCCE was used as an oxygen plasma instrument.



Figure 2.2 : Oxygen Plasma Device

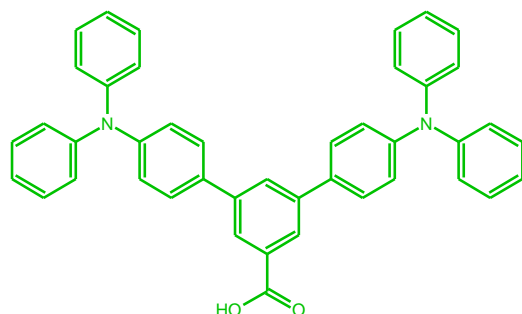
2.3 Surface Treatment of ITO by Using SAM Technique

In this study, two molecules (SAM materials) were designed and ITO substrates were modified with these SAM materials. It is believed that these molecules will increase charge injection and also solve the work function problem between the metal electrode (ITO) and organic layer. These molecules are also known as hole injection materials and which is called triphenylamine. Their chemical structures are shown in Figure 2.2 and their names are; **4,4''-bis(diphenylamino)-1,1':3',1''-terphenyl-5'-carboxylic acid (abbreviated as TPA in this thesis)** and **4,4''-di-9H-carbazol-9-yl-1,1':3',1''-terphenyl-5'-carboxylic acid (abbreviated as CAR in this thesis)**.

By modifying the ITO surface, the band gap between the Fermi energy level of ITO and HOMO energy level of organic material is expected to be decreased. Therefore,

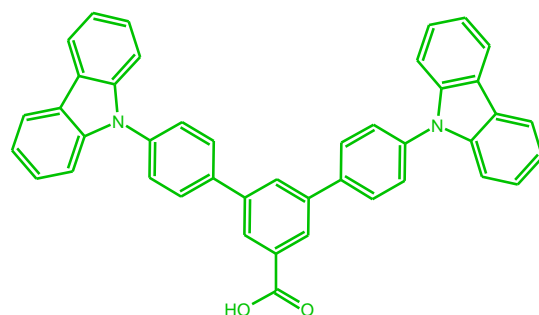
the HOMO energy level of ITO/SAM surface should be determined with Cyclic Voltammetry after ITO was treated with SAM material.

a.



Molecular Formula	= C ₄₃ H ₃₂ N ₂ O ₂
Formula Weight	= 608.7265
Composition	= C(84.84%) H(5.30%) N(4.60%) O(5.26%)
Molar Refractivity	= 190.05 ± 0.3 cm ³
Molar Volume	= 494.8 ± 3.0 cm ³
Parachor	= 1357.9 ± 4.0 cm ³
Index of Refraction	= 1.694 ± 0.02
Surface Tension	= 56.7 ± 3.0 dyne/cm
Density	= 1.230 ± 0.06 g/cm ³
Dielectric Constant	= Not available
Polarizability	= 75.34 ± 0.5 10 ⁻²⁴ cm ³
Monoisotopic Mass	= 608.246378 Da
Nominal Mass	= 608 Da
Average Mass	= 608.741874 Da

b.



Molecular Formula	= C ₄₃ H ₂₈ N ₂ O ₂
Formula Weight	= 604.6947
Composition	= C(85.41%) H(4.67%) N(4.63%) O(5.29%)
Molar Refractivity	= 187.39 ± 0.5 cm ³
Molar Volume	= 482.8 ± 7.0 cm ³
Parachor	= 1301.0 ± 8.0 cm ³
Index of Refraction	= 1.703 ± 0.05
Surface Tension	= 52.6 ± 7.0 dyne/cm
Density	= 1.25 ± 0.1 g/cm ³
Dielectric Constant	= Not available
Polarizability	= 74.29 ± 0.5 10 ⁻²⁴ cm ³
Monoisotopic Mass	= 604.215078 Da
Nominal Mass	= 604 Da
Average Mass	= 604.70997 Da

Figure 2.3 : Chemical structure of TPA (a) and CAR (b) Molecules

Each of these materials was solved in 10⁻³ M dimethyl sulfoxide solution. After dimethyl sulfoxide-SAMs solution was prepared, ITO substrates were kept in these solutions for 24 hours. After 24 hours passed, ITO substrates are rinsed with pure dimethyl sulfoxide to remove the residual SAM molecules which are not having strong bonding on the ITO surfaces. Then ITO substrates were dried with nitrogen (N₂) gas and finally kept on the hot plate for 15 minutes at 80 °C (completely dry ITO substrates).

2.4 Thermal Evaporation of Organic Layers and Metallic Layer

In this study, a thermal evaporation system (NANOVAK) was used for two different coating system. Namely, the system shown in Figure 2.2 is used to coat both organic

and metallic layers. In detail, one of the evaporation is made for small organic molecules like TPD, NPB, Alq₃ etc.. The other evaporation is made for metallic materials like Al, Ag, Au etc. Before starting evaporation, thickness monitors were calibrated and properties of both organic materials (TPD, Alq₃) and metallic material (Al) were entered. Evaporation procedure was completed under high vacuum ($\sim 4 \times 10^{-5}$ Torr) to have high quality thin layers.

TPD and Alq₃ were coated on the SAM modified ITO substrates as HTL and EM, respectively. After organic layers were coated, all of the samples were put into the glove box and cathode layer was coated with aluminum in this inert medium.



Figure 2.4 : Organic (a) and Metallic (b) Evaporation Systems

In this study, six devices were fabricated with SAM materials and the effect of SAM materials was investigated on the electrical and optical characterization of OLED devices with compared to bare ITO OLED device and ITO:PEDOT:PSS OLED device. These device configurations are tabulated in Table 2.1.

Table 2.1 : Configuration of OLED devices

Devices	Transparent Anode	SAM Materials	PEDOT:PSS	Hole Transport Layer	Emissive Layer and ETL	Cathode Layer
Device 1	ITO	-	-	TPD (~40nm)	Alq ₃ (~40nm)	Al (~100nm)
Device 2	ITO	-	PEDOT:PSS	TPD (~40nm)	Alq ₃ (~40nm)	Al (~100nm)
Device 3	ITO	CAR	-	TPD (~40nm)	Alq ₃ (~40nm)	Al (~100nm)
Device 4	ITO	CAR	PEDOT:PSS	TPD (~40nm)	Alq ₃ (~40nm)	Al (~100nm)
Device 5	ITO	TPA	-	TPD (~40nm)	Alq ₃ (~40nm)	Al (~100nm)
Device 6	ITO	TPA	PEDOT:PSS	TPD (~40nm)	Alq ₃ (~40nm)	Al (~100nm)

2.5 Characterization of OLED Devices

Surface topography and electrical characterizations of modified and unmodified ITO were determined by Atomic Force Microscopy (AFM) and Kelvin Probe Force Microscopy (KPFM). For surface topography, AFM was used with non-contact mode. For electrical characterization, KPFM was used with contact and non-contact

mode. Finally, for electrical and optical characterization, Keithley source meter, Labview software, Ocean optic and Spectrometer were used.

2.5.1 AFM surface characterization

Atomic Force Microscope is the most effective instrument for taking nanoscale images of surface topography. In AFM devices usually piezoelectric materials are used as scanning probe because of their high resolution capabilities and fast response time [37].

The general work principle of AFM is illustrated in Figure 2.4. An AFM uses a cantilever with a very sharp tip to scan the sample surface. When cantilever approach to the surface, attractive force occurs between the surface and tip. This force deflects the cantilever. Cantilever deflection usually detected by a laser beam and this laser beam focuses on the top of the cantilever and directs to a position-sensitive photo diode[38]. All of the changes on the surface effect the cantilever deflection and accordingly position of laser change on the photo diode. This changing is recorded by a photo diode to determine surface image.

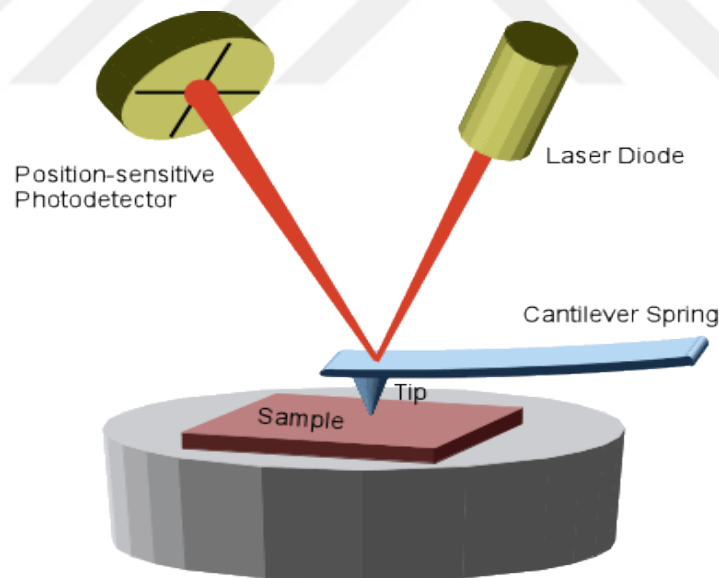


Figure 2.5 : General work principle of AFM (URL 2)

AFM devices usually include three modes. These modes are; contact, non-contact and tapping mode. Selections of these modes are determined according to the surface properties of materials. Generally, contact mode has been used for rigid materials, the non-contact mode has been used for soft materials and tapping mode has been

used for both rigid and soft materials. In addition, the main goal of AFM is determine 3D surface view, lithography and surface roughness [CAN M. 2012].

In this study, Nanosurf flex AFM was used to investigate the surface topography of modified and unmodified ITO. The non-contact mode was used for both of the modified and unmodified ITO measurements. The Figure 2.5 shows Nanosurf flex AFM device and its software screen.

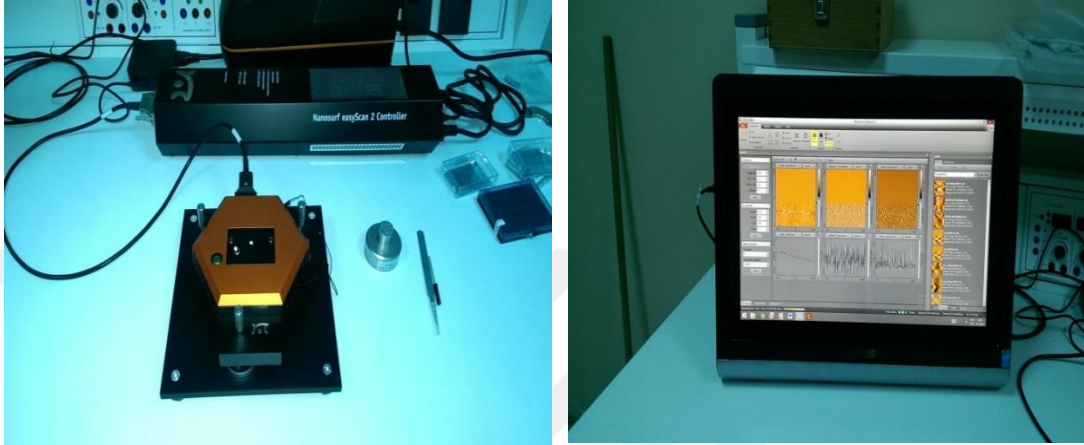


Figure 2.6 : Nanosurf Flex AFM (right) and its software (left)

2.5.2 Kelvin probe force microscopy (KPFM) surface characterization

Kelvin Probe Force Microscopy is usually used to image surface potential difference between the samples and probes. Also it gives details about surface photovoltage of the semiconductors[39]. Thus, it gives information about the work function of conductive thin films.

In KPFM method two conductors have been used as parallel plate capacitor. The contact potential difference between (V_{CPD}) of two materials are defined as in Equation 2.1.

$$V_{CPD} = \frac{1}{e(\phi_2 - \phi_1)} \quad (2.1)$$

Where ϕ_2 and ϕ_1 are work function of conductors. Due to the distance between parallel plate capacitor, a periodic vibration of distance (ω) is occurred. This vibration causes a current and this current equation is written as follows,

$$i(t) = V_{CPD} \omega \Delta C \cos \omega t \quad (2.2)$$

where ΔC is the change in the capacitance. For measuring V_{CPD} , voltage is applied between two plates until current $i(t)$ goes to zero[40].

In this study, Ntegra Solaris (NT-MDT) KPFM was used to determine the surface potential difference between the modified and unmodified ITO.

2.5.3 Cyclic voltammetry characterization

Cyclic Voltammetry (CV) is used in electrochemistry, inorganic chemistry, organic chemistry and biochemistry. It consists of cycling the potential of an electrode. This electrode dips in a solution and measures the current. The potential of this working electrode is controlled by a reference electrode. Silver (Ag) or silver chloride (AgCl) usually used as reference electrode [41].

The potential is applied between the working electrode and the reference electrode. Where, the current is measured between the working electrode and the counter electrode. These data gives current versus applied potential graph. This graph is referred as voltammogram. The Figure 2.6 shows a current versus potential voltammogram.

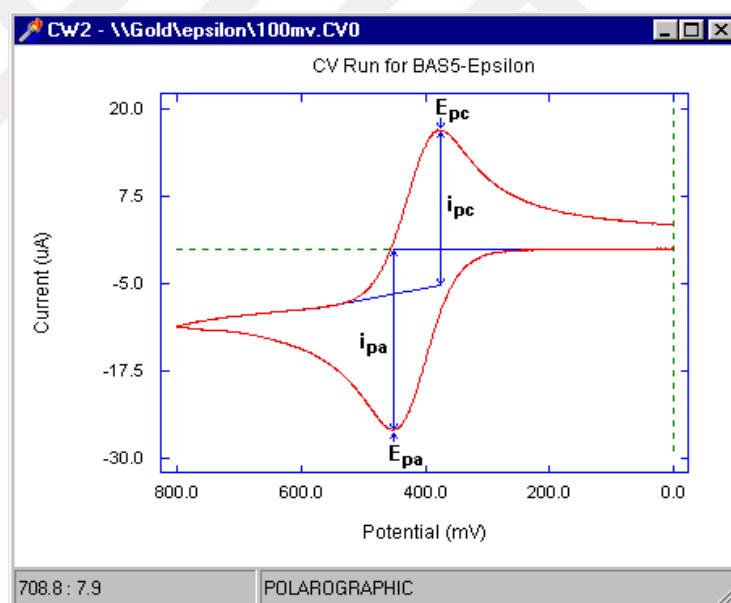


Figure 2.7 : Typical current vs potential graph of CV

2.5.4 Contact angle characterization

The contact angle measurement technique is usually used to determine whether a solid surface is hydrophobic or hydrophilic. Generally, this is explained as follows. If a contact angle is less than 90° , solid surface is considered as hydrophilic and the fluid is spread over a large area of surface. If the contact angle is larger than 90° it means that solid surface is hydrophobic and the fluid minimize its contact with the

surface[42]. The Figure 2.7 shows that if the liquid spreads on the surface, a small contact angle is observed. If the liquid beads on surface, a large contact angle is observed.

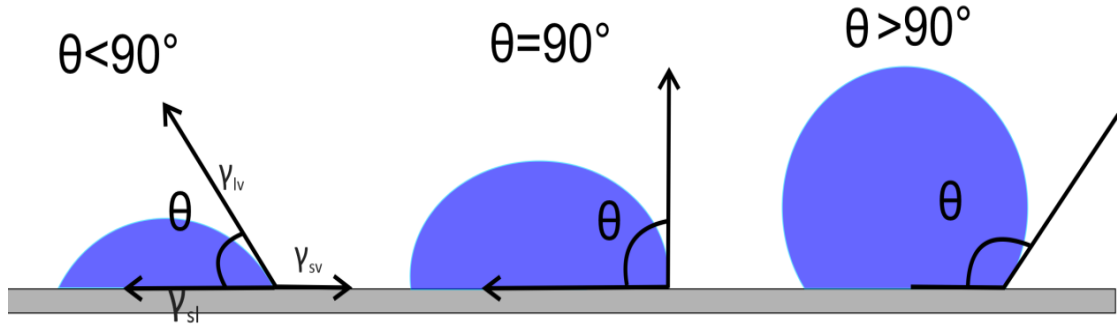


Figure 2.8 : Illustration of contact angles on a smooth solid surface.

Generally, measurement of contact angles on a solid surface is the easiest way to determine the surface energetics (solid-vapor and solid-liquid surface tensions). It is obtained by Young's equation as follows,

$$\gamma_{lv} \cos \theta = \gamma_{sv} - \gamma_{sl} \quad (2.3)$$

where θ , γ_{lv} , γ_{sv} and γ_{sl} are Young contact angle, liquid-vapor surface tension, solid-vapor surface tension and solid- liquid surface tension, respectively[43].

2.5.5. Optical and electrical characterization

To obtain current-voltage (I-V) characteristic of OLED devices, Keithley 2400 source meter was used. Voltage was applied between the anode and cathode with two probes of Keithley source meter and LabView software was used to obtain I-V characteristic of OLED on a computer screen.

In order to obtain optical properties of OLED devices QE6500 spectrometer was used.

3. RESULT AND DISCUSSION

PEDOT:PSS which is coated on ITO has been used most effective hole injection material in organic light emitting diode. But according to many researches, ITO/PEDOT:PSS interface is not stable and some degradation has been occurred on ITO surface. The degradation reason of ITO can be explained by etching of ITO due to the strong acidic nature of PEDOT:PSS. Because it is known that ITO is very sensitive to acidic environments and therefore it influences device life time negatively[44, 45]. Because of this problem self-assembled monolayers was used which is an alternative material as hole injection layer instead of PEDOT:PSS. In addition, the effect of self-assembled monolayer on OLEDs device was discussed in the preceding parts.

This chapter includes six parts and in these parts; electrical, optical and surface characterization of modified and unmodified ITO was analyzed. In the first three section modified ITO with SAM materials were compared to unmodified ITO and modified ITO with PEDOT:PSS via their electrical and optical characterization. In the fourth part, surface characterization of modified and unmodified ITO was performed with AFM and KPFM. In the fifth part, electrical characterization of SAM materials (CAR-TPA) was analyzed with Cyclic Voltammetry and in the last part, modified and unmodified ITO surface was analyzed with contact angle measurement.

3.1 Electrical and Optical Characterization Results

3.1.1 Cycle voltammetry results

In this study, CH instruments CHI440B cyclic Voltammetry was used to determine the electrochemical behavior of SAM (TPA-CAR) materials. Modified ITO with SAM materials, platinum wire and silver (Ag) were used as working electrode, counter electrode and a reference electrode respectively. Before starting the measuring process, nitrogen gas has been used to remove oxygen from the electrolyte.

The Figure 3.1 and Figure 3.2 show CV voltammogram of 'TPA and CAR' SAM materials. The energy level of E_{HOMO} was found from the inflection point of these graphs by using Equation 3.2. Using Equation 3.1 and Equation 3.2 values of E_{LUMO} and E_{HOMO} can be calculated.

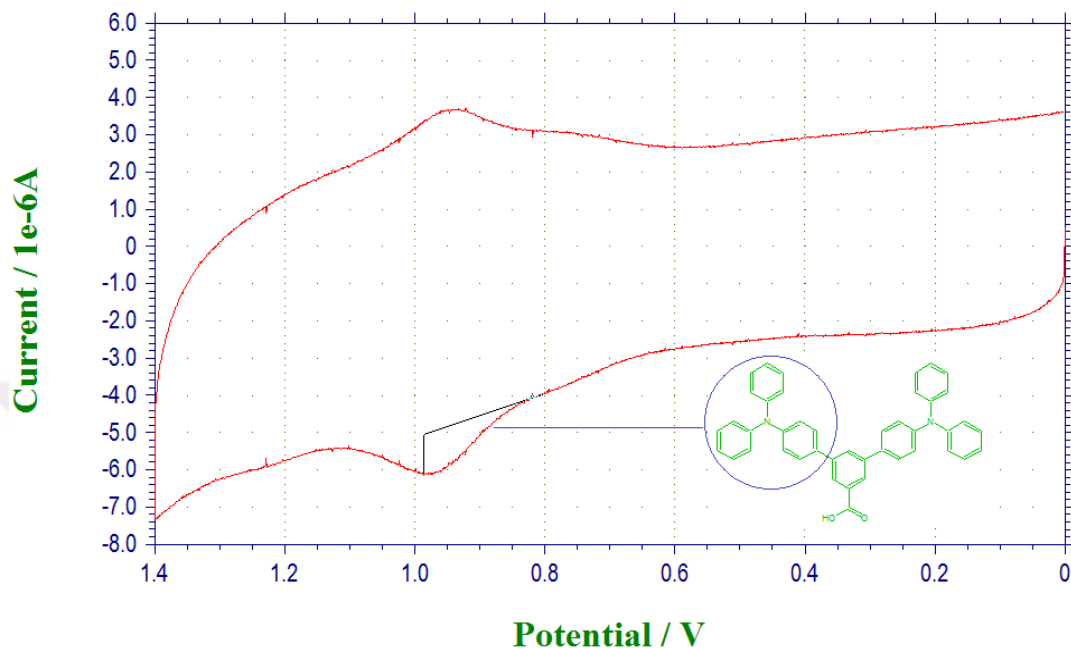


Figure 3.1 : CV Voltammogram of modified ITO with TPA

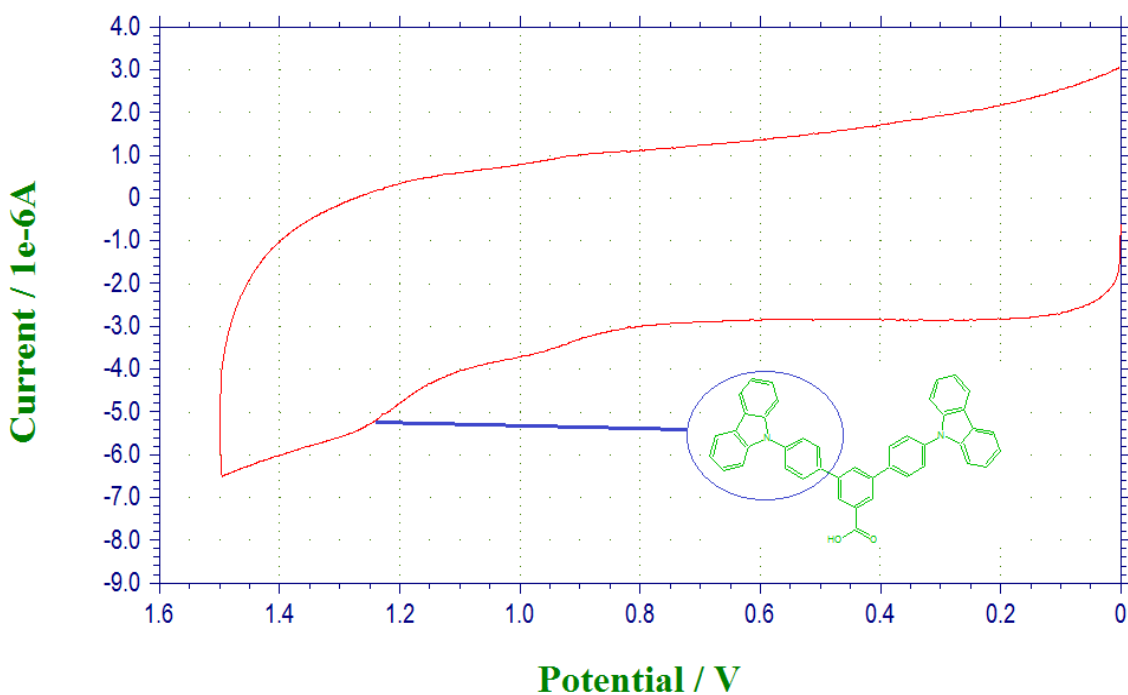


Figure 3.2 : CV Voltammogram of modified ITO with CAR

$$E_{\text{LUMO}} = -e(E_{1/2(\text{ind.})} + 4,4) \quad (3.1)$$

$$E_{\text{HOMO}} = -e(E_{1/2(\text{yük.})} + 4,4) \quad (3.2)$$

As shown in Figure 3.1 and Figure 3.2 reversible oxidation of TPA and semi reversible oxidation of CAR was determined 0,92 V and 1,18 V, respectively. HOMO energy level of TPA and CAR were calculated using Equation 3.2. This energy level was founded as -5,32 eV and -5,58 eV for TPA and CAR, respectively.

The effect of SAM materials on the ITO surface can be seen in the energy diagram of devices given in Figure 3.3. As it will be understood from the figure both TPA and CAR increase the energy level of ITO. Nevertheless, TPA is more suitable for ITO and TPD, because it makes an energy step between the ITO and TPD. Therefore, devices which are modified with TPA should have better electrical and optical results.

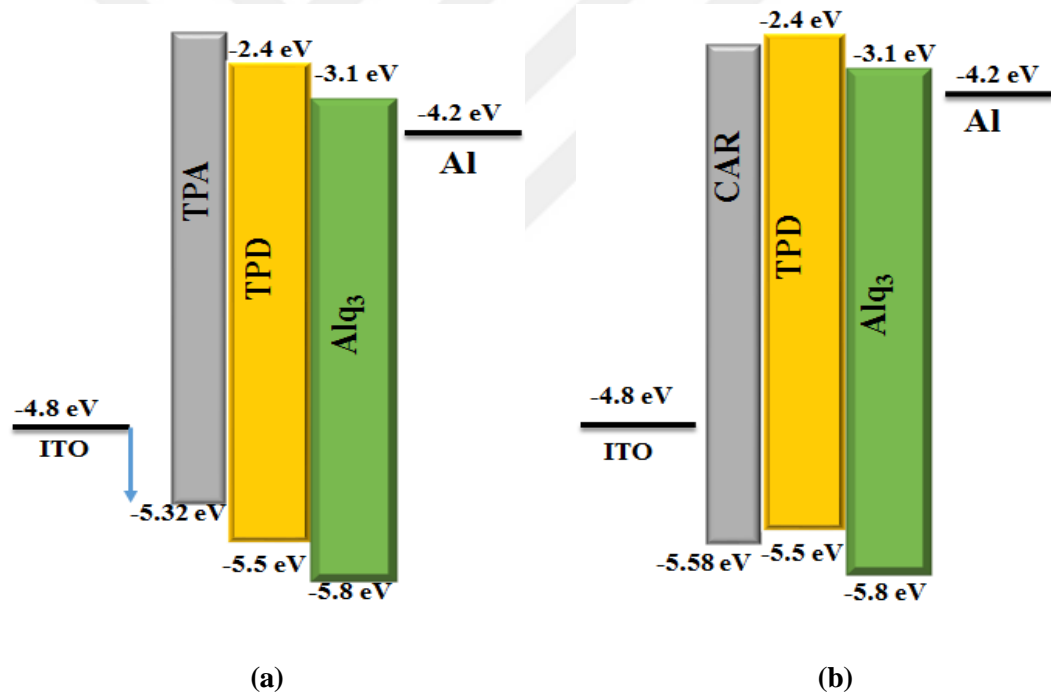


Figure 3.3 : Energy diagram of OLED devices with TPA (a) and CAR (b)

3.1.2 Electrical and optical characterization of 4,4''-di-9H-carbazol-9-yl-1,1':3',1''-terphenyl-5'-carboxylic acid (CAR)

To determine the effect of ITO surface treatment on OLED device performance, six different device structures were prepared. Then, the manufactured OLEDs are compared via their electrical and optical properties. In this section, ITO was modified with CAR, PEDOT:PSS and CAR/PEDOT:PSS. These modified ITO

devices (ITO/CAR and ITO/CAR/PEDOT:PSS) were compared with reference devices (Bare ITO and ITO/PEDOT:PSS). Detailed device numbers and structures are given in Table 3.1.

Table 3.1 : Device numbers and their structures

Device 1	Device 2	Device 3	Device 4
ITO/TPD/Alq ₃ /Al	ITO/PEDOT:PSS/TPD/Alq ₃ /Al	ITO/CAR/TPD/Alq ₃ /Al	ITO/CAR/PEDOT:PSS/TPD/Alq ₃ /Al

I-V characteristic curves show the relationship between the current flowing through the electronic device and applied voltage across its terminals. It is the most important electrical property for an organic light emitting diode. By means of this characterization, one can determine if really a diode is manufactured or not. The Figure 3.4 shows J-V curves of Device 1,2,3 and 4. As known, semiconductor diodes begin conducting electricity only if a certain threshold voltage or cut-in voltage is present in forward bias and we expect to see this behavior in J-V graph.

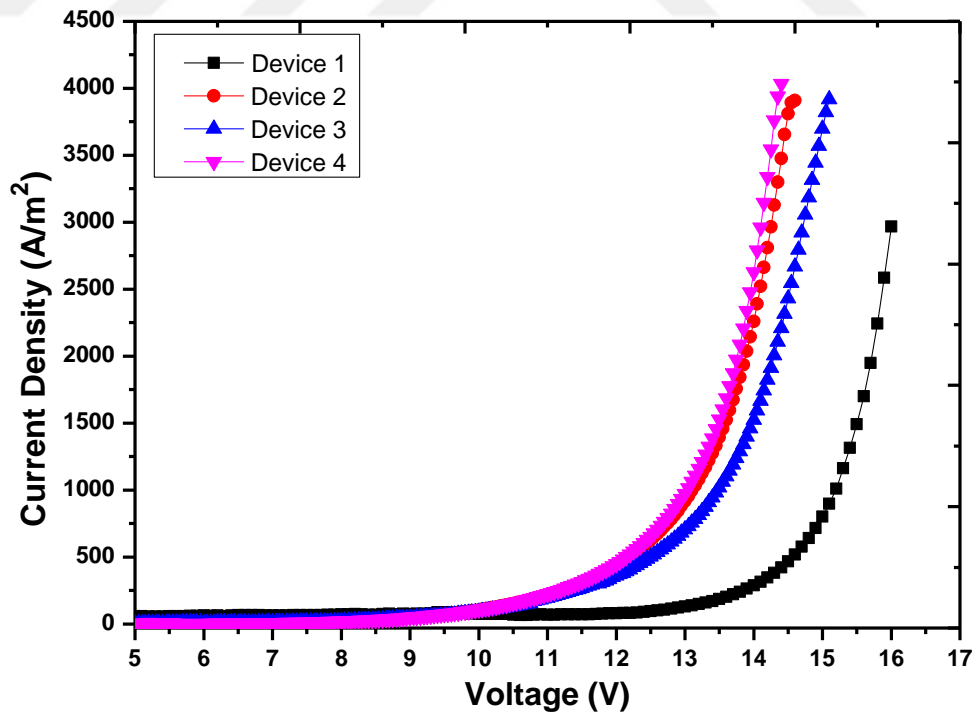


Figure 3.4 : J-V Characteristic of Device 1 to 4

The Figure 3.4 shows a perfect I-V diode characteristic. Device 1,2 and 3 are not conducting electricity until they are applied $\sim 8,2$ volts and $\sim 12,5$ volts for Device 4. After $\sim 8,2$ and $\sim 12,5$ volts is applied, devices start to conduct electricity. We refer that voltages (8,2 and 12,5) as a turn on voltage. In Device 1,2 and 3 modified ITO was used and these devices show a low turn on voltage compared to Device 4 which uses a bare ITO. The detailed structure of all devices can be seen in Table 3.1.

In OLEDs, electrical energy is converted into optical energy. This feature shows there is a direct relationship between the voltage-current and luminance. In addition, this means that the luminance has a key point for optical properties of OLEDs. The Figure 3.5 shows luminance change versus voltage of Device 1 to 4.

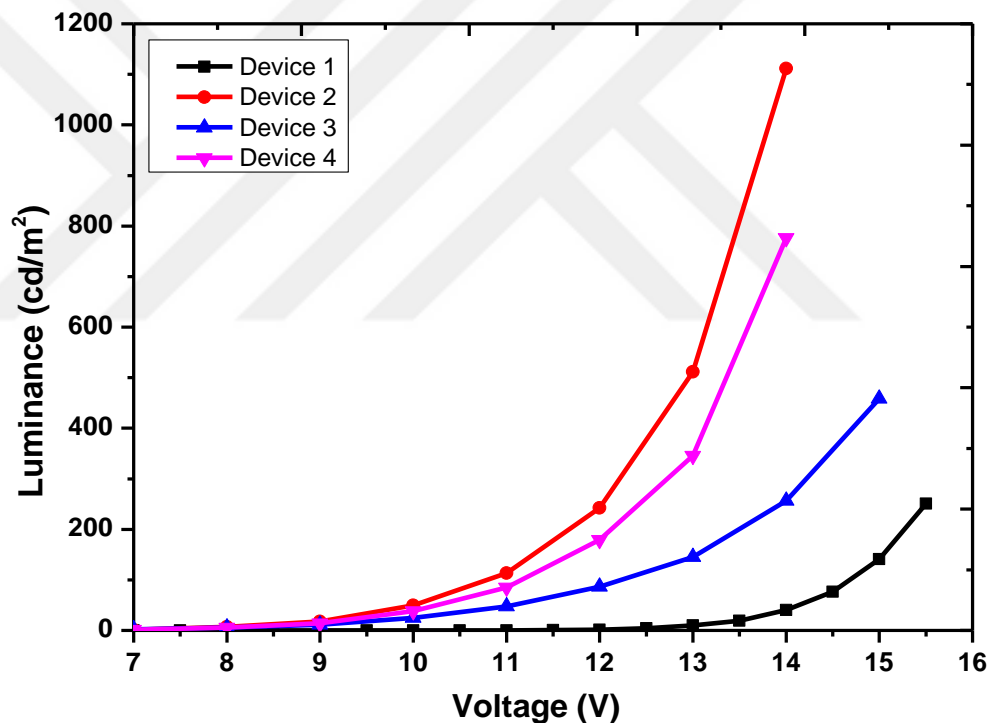


Figure 3.5 : Luminance versus Voltage graph of Device 1 to 4

If Figure 3.4 and Figure 3.5 clearly compares, the relationship between electrical and optical behavior of OLEDs. In Figure 3.4 turn on voltage of Device 1, 2 and 3 are about 8,2 V and Device 4 is about 12,5 V. In the same way Device 1,2,3, and 4 gives the luminance at the same turn on voltage (Figure 3.5). As expected, Device 2 with ITO/PEDOT:PSS has maximum luminance, Device 3 and 4 with ITO/CAR and ITO/CAR/PEDOT:PSS show good performance according to Device 1. As can be

seen in Figure 3.4 and Figure 3.5 CAR material has good result on device performance. Because, it is solved the contact problem between ITO electrode and organic layers.

After current, voltage and luminance of devices are determined, the efficiency of OLED devices can be calculated. Figure 3.6 and figure 3.7 show current and power efficiency of device 1,2,3 and 4, respectively. Here, current efficiency is convenient for quantifying the properties of OLEDs for display applications and Power efficiency is the ratio luminous power emitted in the forward direction[33].

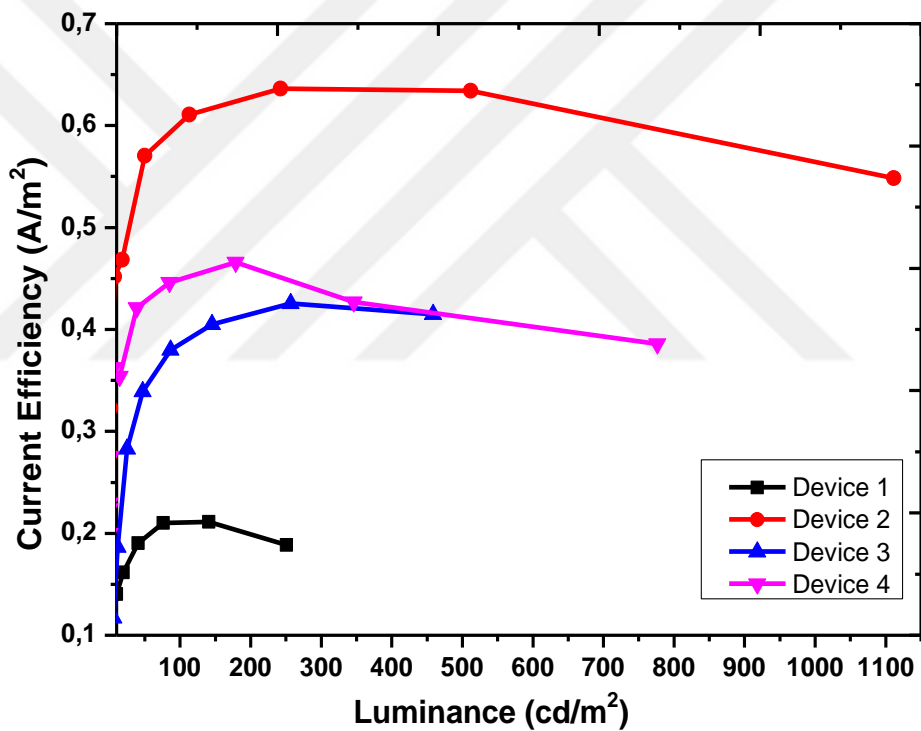


Figure 3.6 : Current Efficiency vs Luminance graph of Device 1 to 4

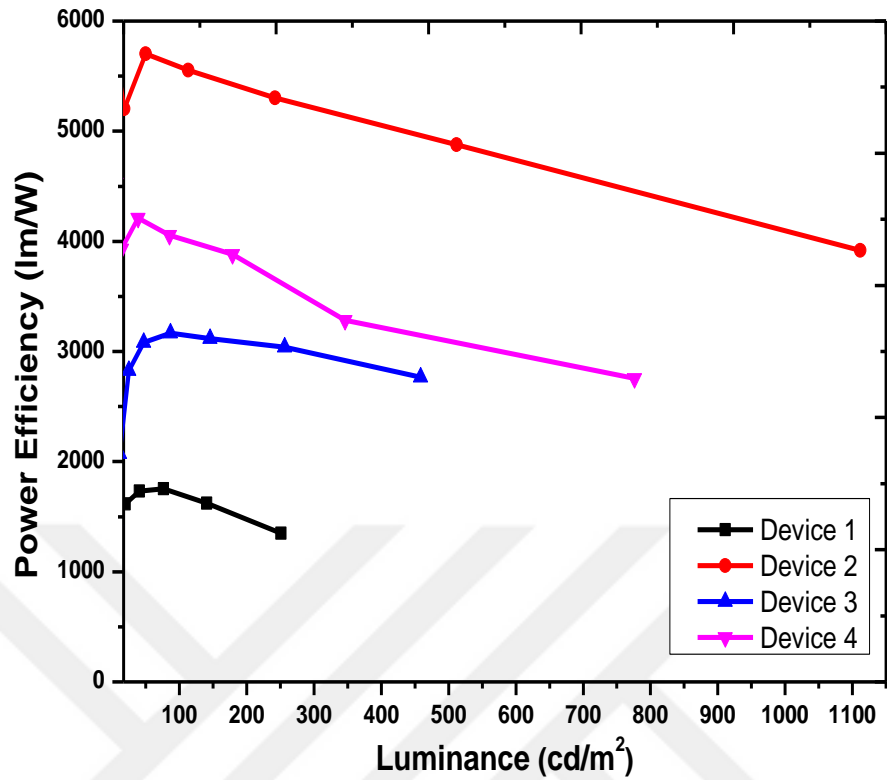


Figure 3.7 : Power Efficiency vs Luminance graph of Device 1 to 4

The Figure 3.8 shows the intensity (a.u) versus wavelength (nm) graph. As can be seen in the figure, all devices emit light almost at the same wavelength. In addition, all devices have maximum intensity at the same wavelength. It means that, recombination of electrons and holes were occurred in emissive layer.

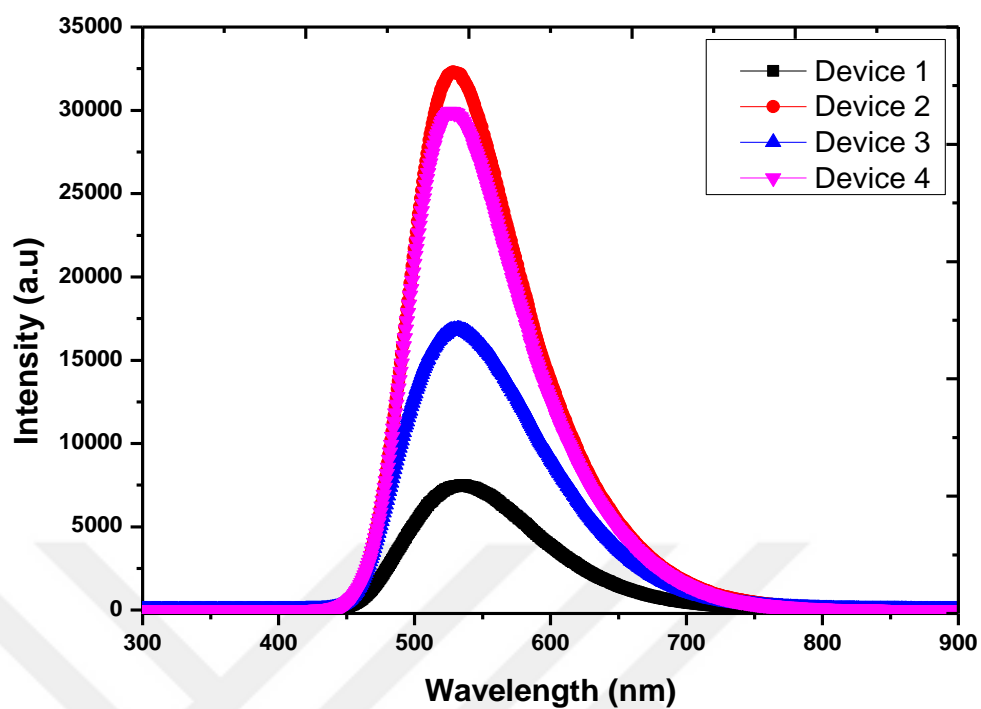


Figure 3.8 : Intensity vs Wavelength graph for Device 1 to 4

Table 3.2 : Electrical and Optical details about devices

	Turn on Vol. (V)	Max. Lum. (cd/m ²)	Max. Current Effi. (cd/A)	Max. Power Effi. (lm/W)
Device 1	12,5	250,7	0,211	1753
Device 2	8,0	1111,5	0,636	5702
Device 3	8,2	458,6	0,426	3166
Device 4	8,1	776,4	0,466	4211

3.1.3 Electrical and optical characterization of 4,4''-bis(diphenylamino)-1,1':3,1''-terphenyl-5'-carboxylic acid (TPA)

In this section, four different devices were prepared and the corresponding structures and their abbreviated names are tabulated in Table 3.3.

Table 3.3: Device structures and their numbers

Device 1	Device 2	Device 5	Device 6
ITO/TPD/Alq ₃ /Al	ITO/PEDOT:PSS/TPD/Alq ₃ /Al	ITO/TPA/TPD/Alq ₃ /Al	ITO/TPA/PEDOT:PSS/TPD/Alq ₃ /Al

As can be seen in Table 3.3 ITO was modified with TPA and TPA/PEDOT:PSS for Device 5 and Device 6, respectively. These devices were compared to reference devices (Device 1 and Device 2) via their electrical and optical characterization.

In the previous section, the electrical and optical characterization of OLED device was explained. Hence, brief information is given in the related graphs. First of all, current-voltage and luminance-voltage graphs and then current, power efficiency and intensity versus wavelength graphs are given in Figure 3.9, Figure 3.10, Figure 3.11, Figure 3.12 and Figure 3.13, respectively.

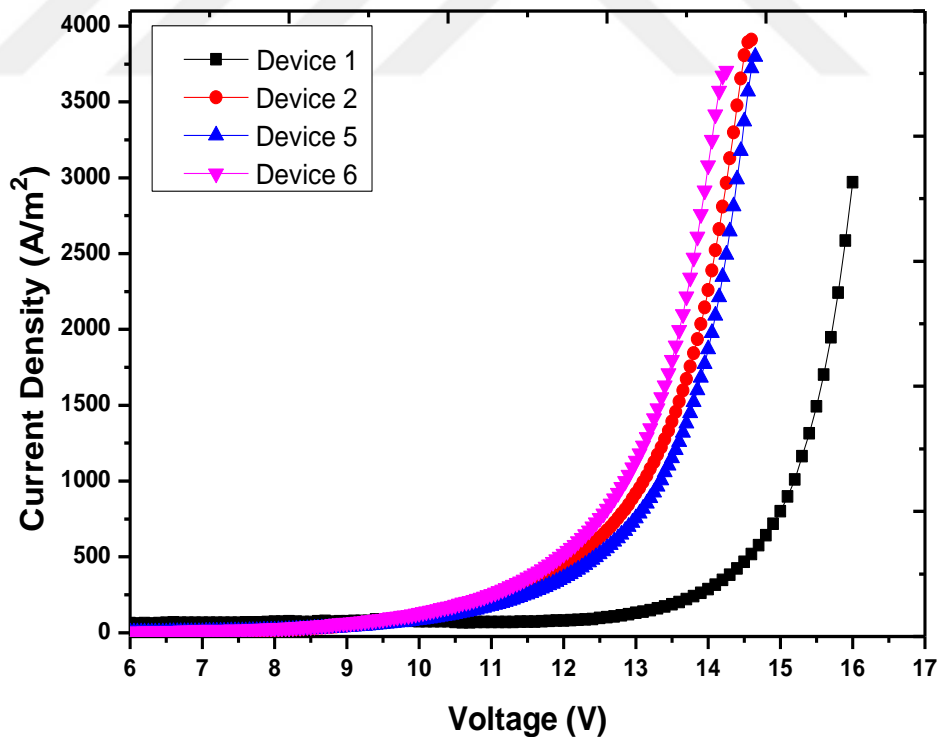


Figure 3.9 : Current Density versus Voltage graph

As can be seen in Figure 3.9, Device 5 and Device 6 have the same turn on voltage with reference Device 2 and also they show a good performance with respect to reference Device 1. Also, Figure 3.9 (electrical characterization) and Figure 3.10 (optical characterization) shows similar features.

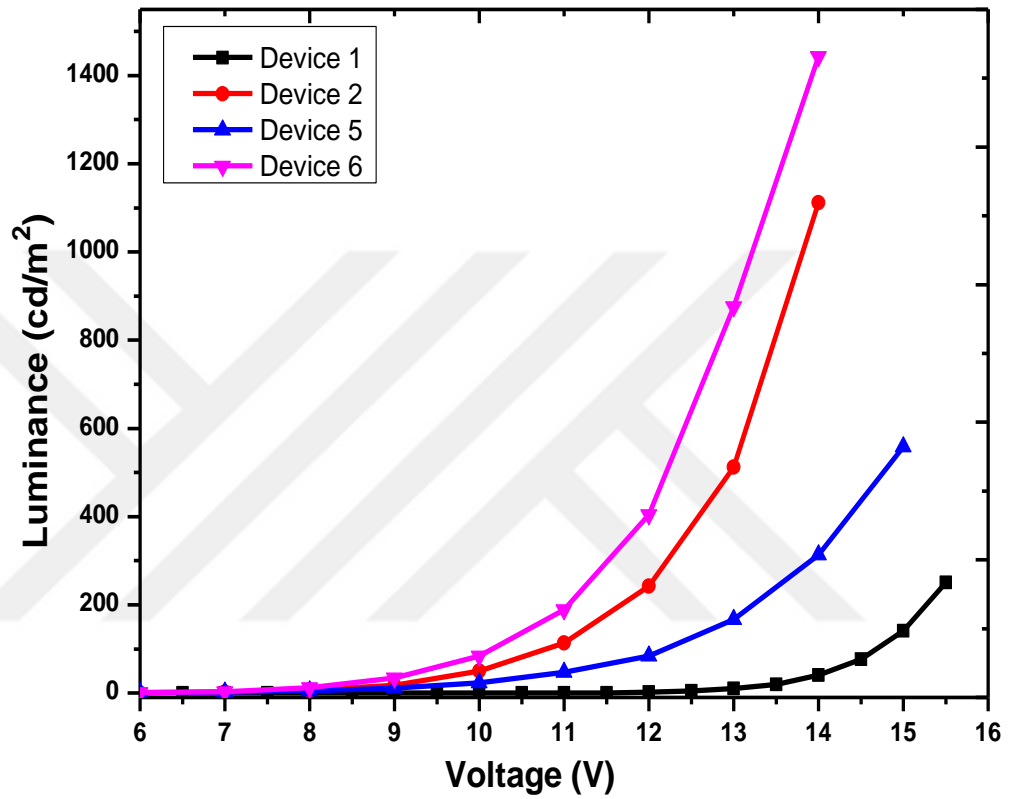


Figure 3.10 : Luminance versus Voltage graph

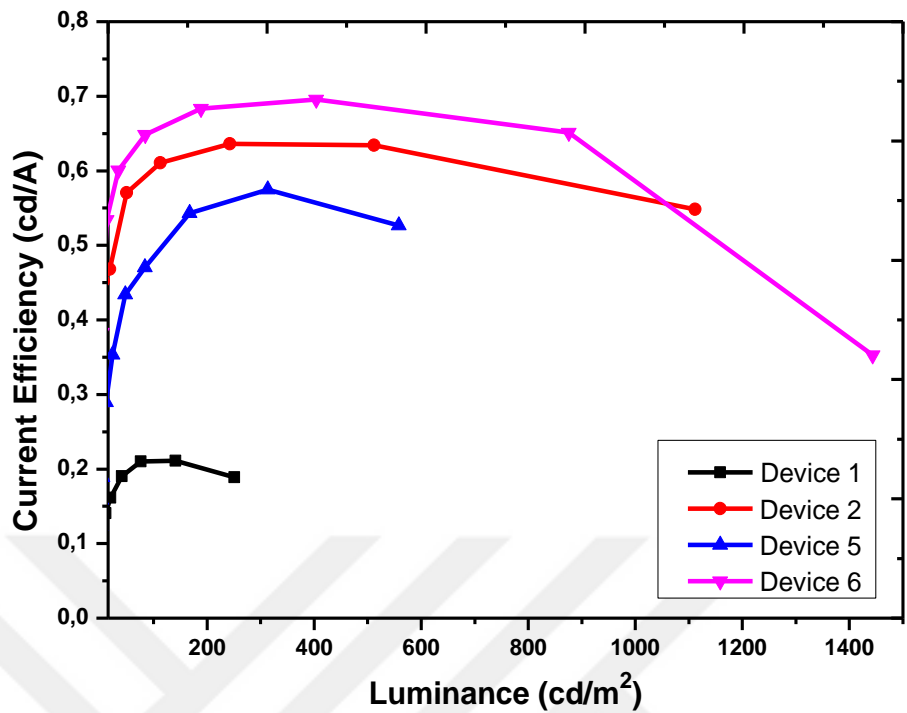


Figure 3.11 : Current Efficiency versus Luminance graph

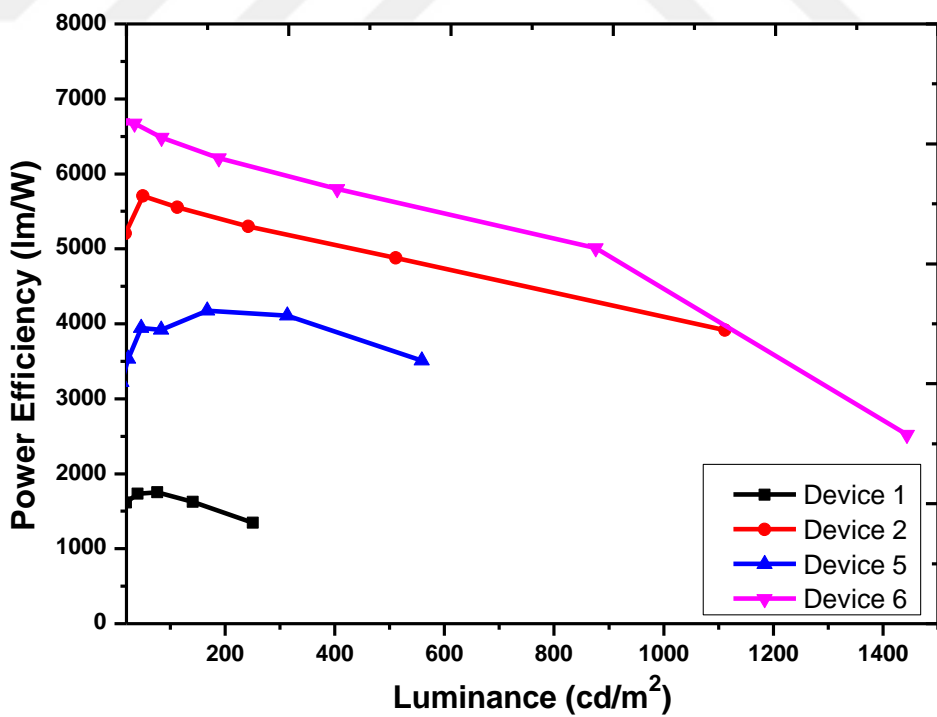


Figure 3.12 : Power Efficiency versus Luminance graph

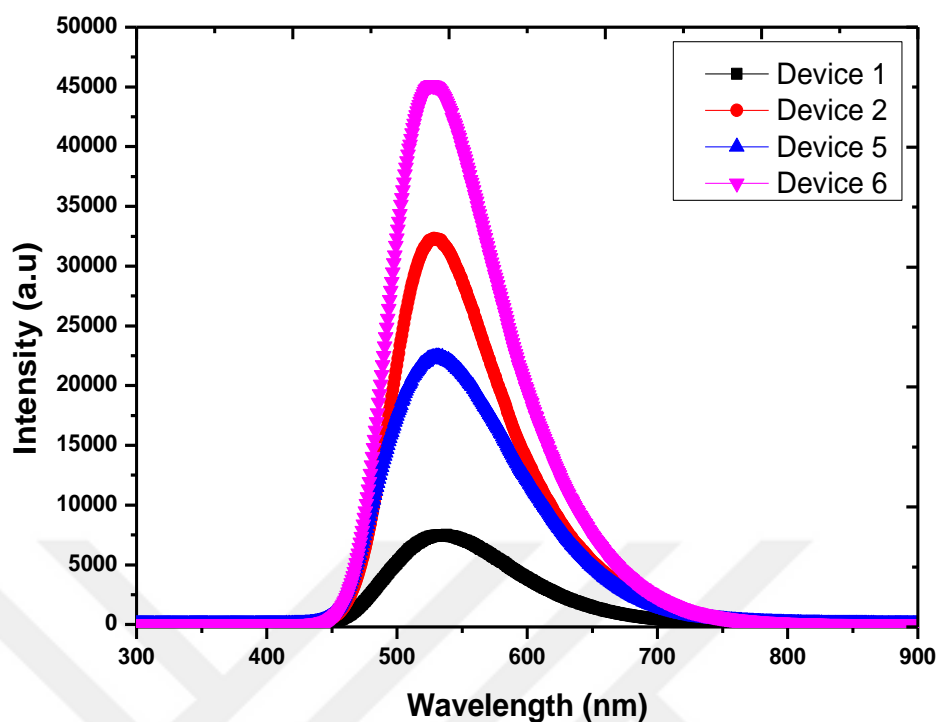


Figure 3.13 : Intensity versus Wavelength Graph

Table 3.4 : Electrical and Optical details about devices.

	Turn on Vol. (V)	Max. Lum. (cd/m ²)	Max. Current Effi. (cd/A)	Max. Power Effi. (lm/W)
Device 1	12,5	250,7	0,211	1753
Device 2	8,0	1111,5	0,636	5702
Device 5	8.3	558,5	0,575	4175
Device 6	8,0	1443	0,696	6678

3.1.4 Electrical and optical characterization of ‘TPA and CAR’ materials

In this part, also the last part of electrical and optical characterization, all of the devices were compared with each other. In the previous section (Section 3.1.2 and 3.1.3.), we compared devices which include CAR and TPA treated ITO with reference devices (Device 1 and Device 2). In this section, the devices which are fabricated with SAM (CAR-TPA) treated ITO were compared with reference devices

and also they are compared with each other, again. Device numbers and structures were given in table 3.5.

Table 3.5 : Device numbers and structures

Device Numbers	Device Structures	Device Numbers	Device Structures
Device 1	ITO/TPD/Alq ₃ /Al	Device 4	ITO/CAR/PEDOT:PSS/TPD/Alq ₃ /Al
Device 2	ITO/PEDOT:PSS/TPD/Alq ₃ /Al	Device 5	ITO/TPA/TPD/Alq ₃ /Al
Device 3	ITO/CAR/TPD/Alq ₃ /Al	Device 6	ITO/TPA/PEDOT:PSS/TPD/Alq ₃ /Al

In section 3.1.1 HOMO level of TPA and CAR was found with cyclic Voltammetry. According to CV results, Device 5 which is modified with TPA should show better performance than Device 3. Because Device 3 includes modified ITO with CAR and its HOMO energy level (Figure 3.3) is not as suitable as a TPA HOMO energy level for ITO and TPD.

SAM materials may not be completely covered on the ITO surfaces. Therefore, PEDOT:PSS was coated on TPA and CAR (Device 4 and Device 6) to observe changing in device performance and observing stability of SAM materials. As expected, Device 4 and Device 6 show better performance than Device 3 and Device 5. This performance change can be seen in Figure 3.14, Figure 3.15, Figure 3.16, Figure 3.17 and Figure 3.18 where the electrical and optical behavior of devices are compared from these graphics, it can be seen that all devices are compatible with each other.

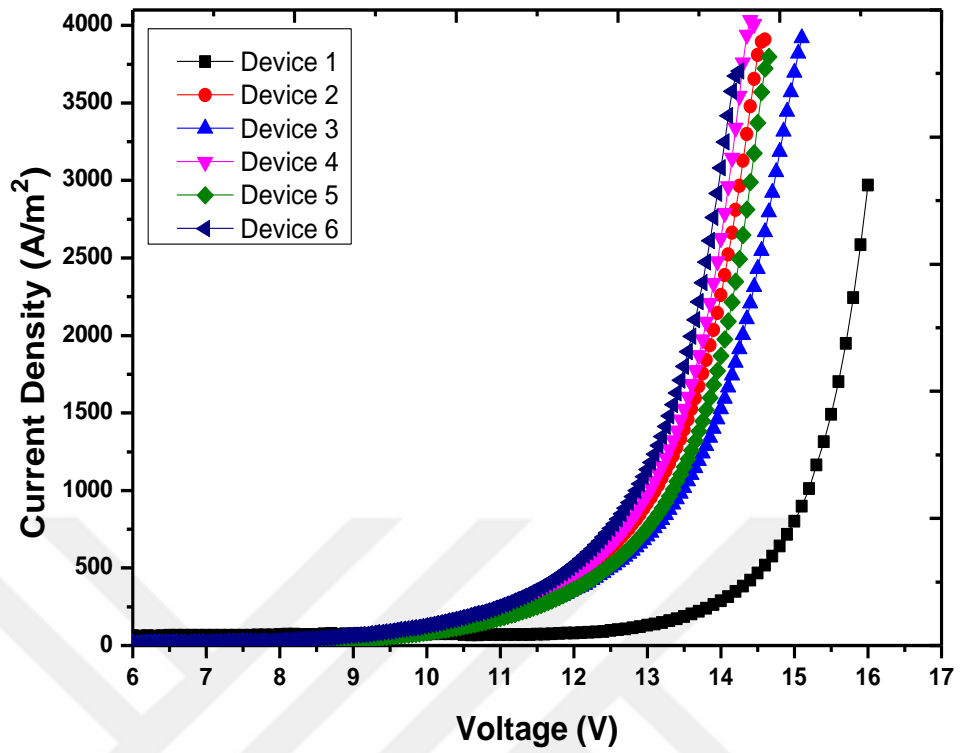


Figure 3.14 : Current Density versus Voltage graph

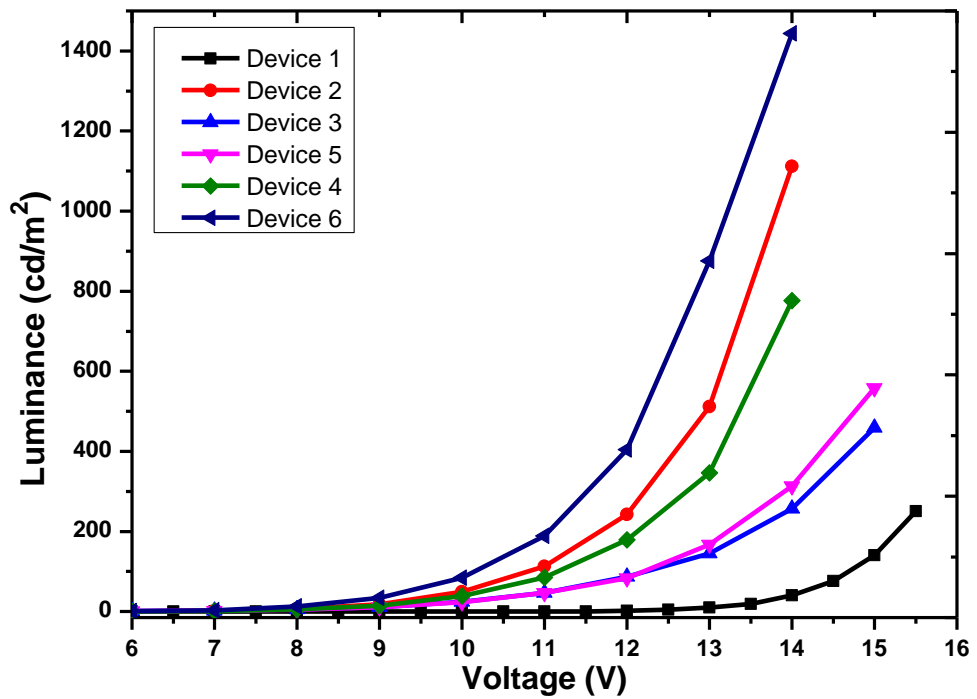


Figure 3.15 : Luminance versus Voltage graph

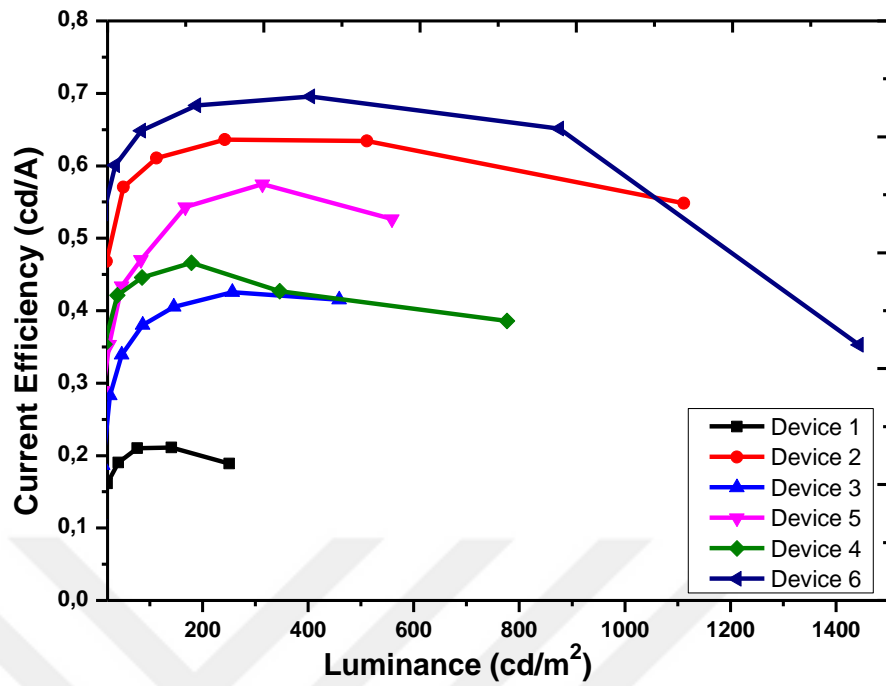


Figure 3.16 : Current Efficiency versus Luminance graph

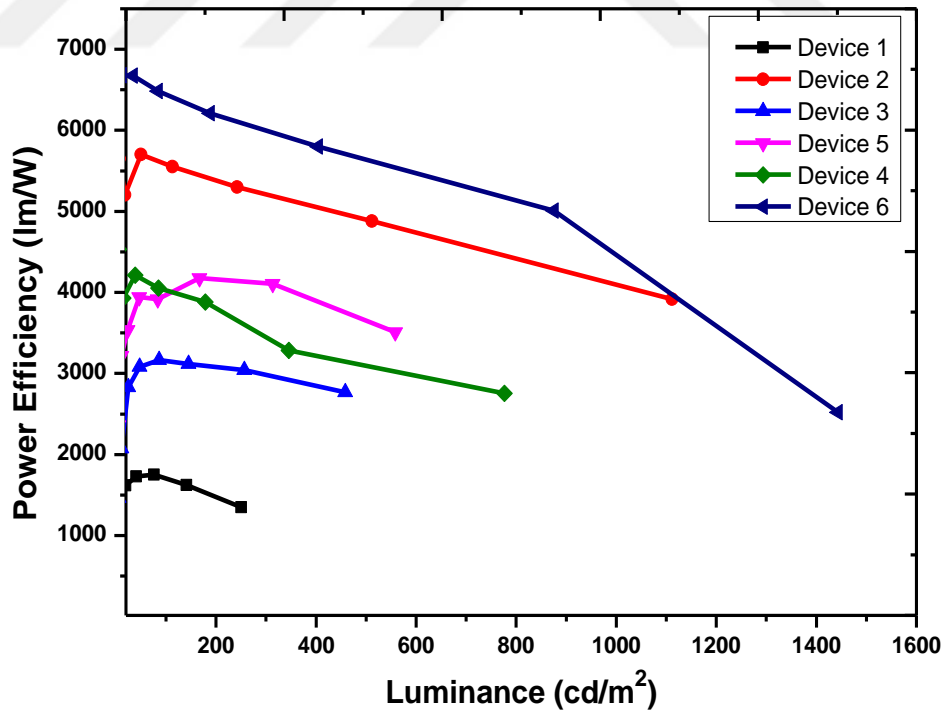


Figure 3.17 : Power Efficiency versus Luminance graph

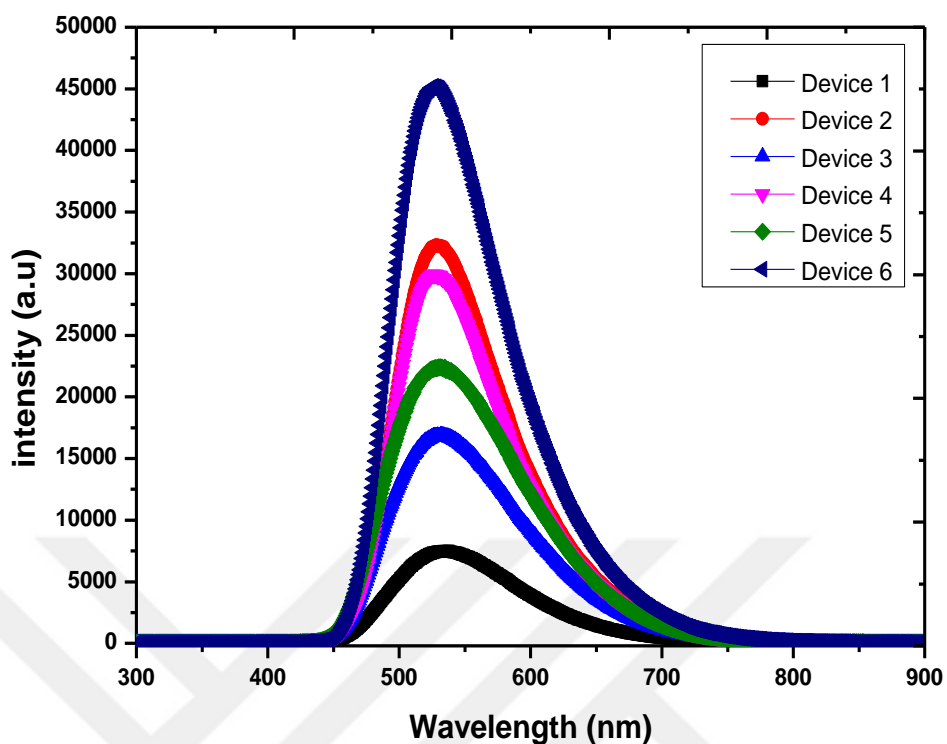


Figure 3.18 : Intensity versus Wavelength graph

Table 3.6 : Electrical and Optical details about devices

	Turn on Vol. (V)	Max. Lum. (cd/m ²)	Max. Current Effi. (cd/A)	Max. Power Effi. (lm/W)
Device 1	12,5	250,7	0,211	1753
Device 2	8,0	1111,5	0,636	5702
Device 3	8,2	458,6	0,426	3166
Device 4	8,1	776,4	0,466	4211
Device 5	8.3	558,5	0,575	4175
Device 6	8,0	1443	0,696	6678

3.2 Surface Characterization Results

3.2.1 Atomic force microscope results

The surface topography of modified and unmodified ITO was characterized by AFM and the AFM images were shown in figure 3.19. As it is widely known, SAM materials have nanoscale size, hence it is too difficult to observe them on ITO surface. However, surface roughness (RMS) measurement differences will give some information about modification of ITO surface with TPA and CAR SAM materials. The results of surface roughness are given in Table 3.7.

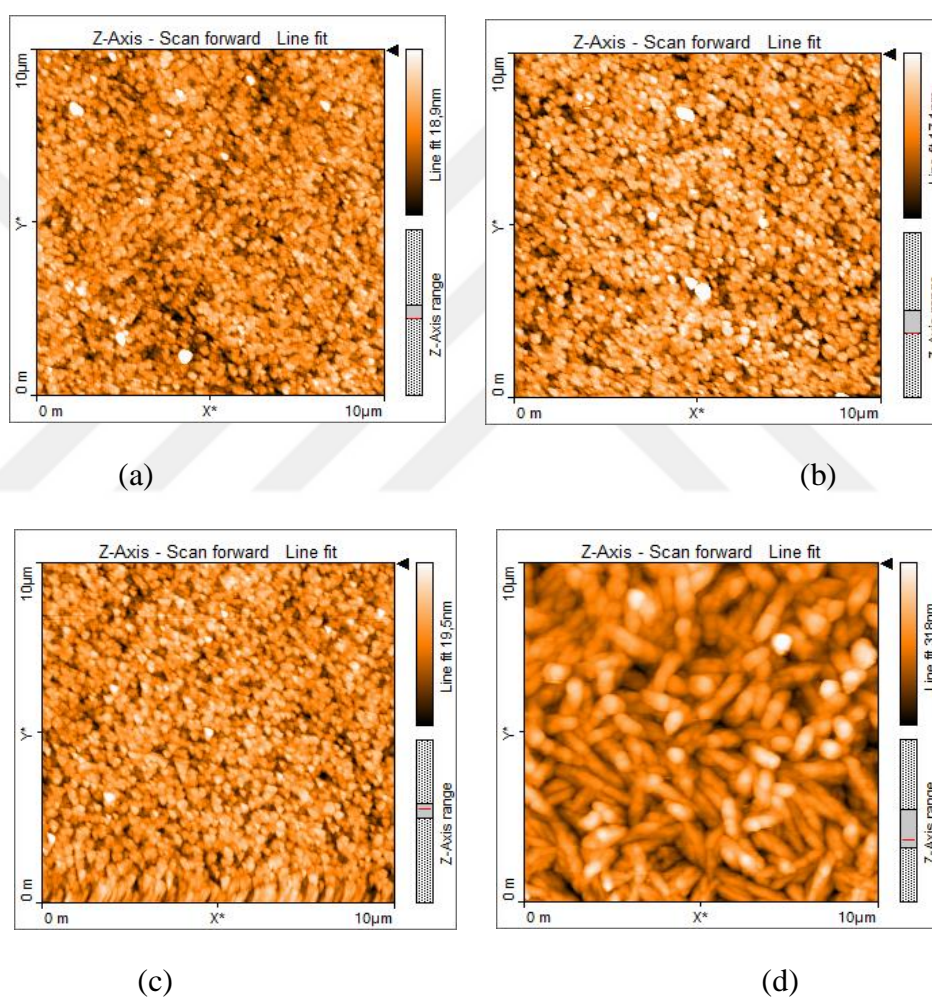


Figure 3.19 : AFM images of Bare ITO (a), modified ITO with CAR (b) and TPA (c). After organic materials coating on ITO (d)

Table 3.7 : Surface roughness of Bare ITO, ITO/CAR, ITO/TPA and ITO/TPD/Alq₃

	Bare ITO	ITO/CAR	ITO/TPA	ITO/TPD/Alq ₃
RMS	4,3 nm	3,9 nm	3,4 nm	48,4 nm

Unmodified ITO has a higher surface roughness than modified ITO with CAR and TPA. It can be said that, SAM materials were covered on ITO surface and filling the vacancies or holes. That process decreases the roughness of ITO.

3.2.2 Kelvin probe force microscope results

In order to determine the surface potential of modified and unmodified ITO Kelvin Probe Force Microscope was used. With this technique, we obtained surface topography images and surface potential topography images. These images are shown as in following Figure 3.20, Figure 3.21 and Figure 3.22.

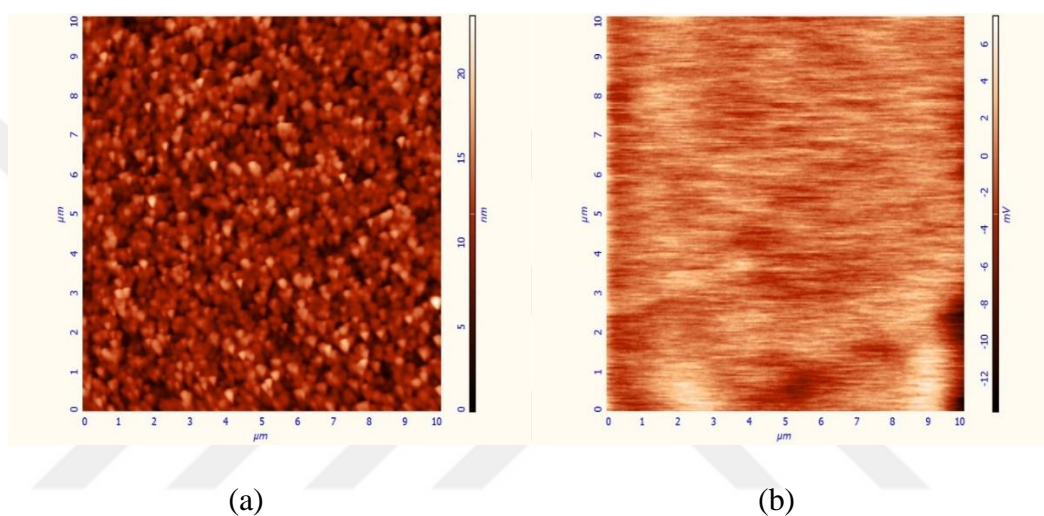


Figure 3.20: AFM topography (a) and surface potential (b) of bare ITO with KPFM technique.

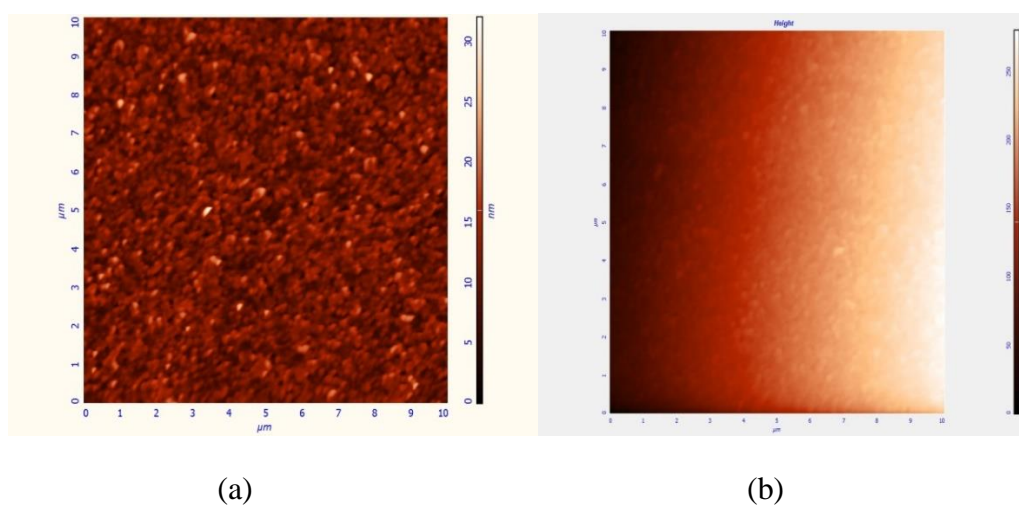
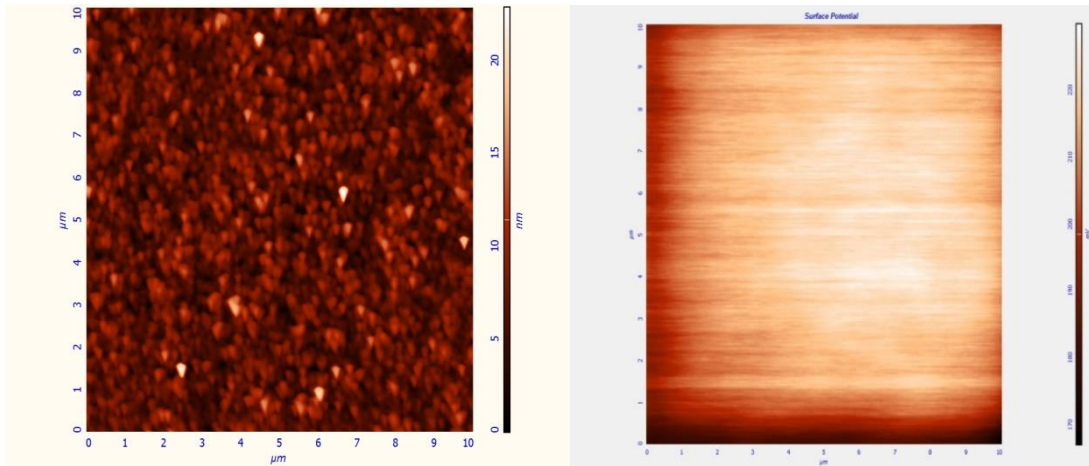


Figure 3.21 : AFM topography (a) and surface potential (b) of ITO/CAR with KPFM technique



(a)

(b)

Figure 3.22 : AFM topography (a) and surface potential (b) of ITO/TPA with KPFM technique

The Figure 3.20 shows the surface potential of bare ITO and modified ITO with CAR and TPA results which is measured with KPFM.

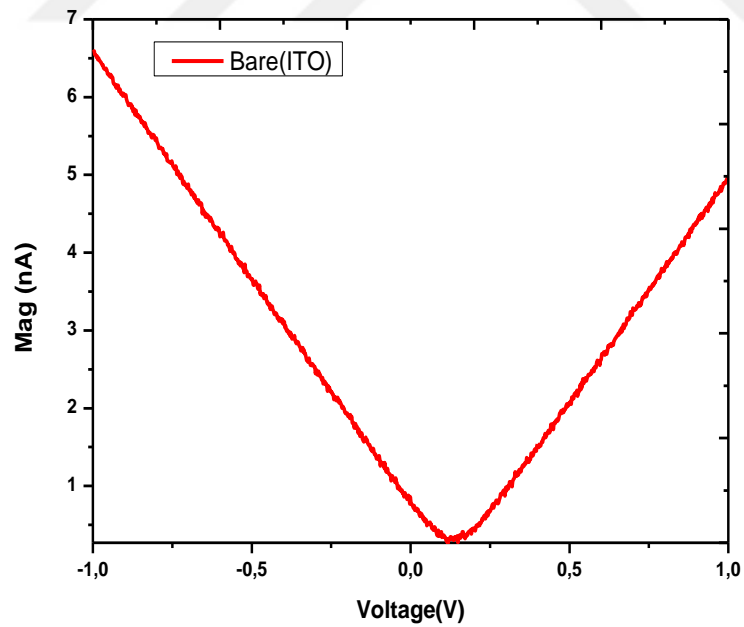


Figure 3.23 : Surface Potential of Bare ITO

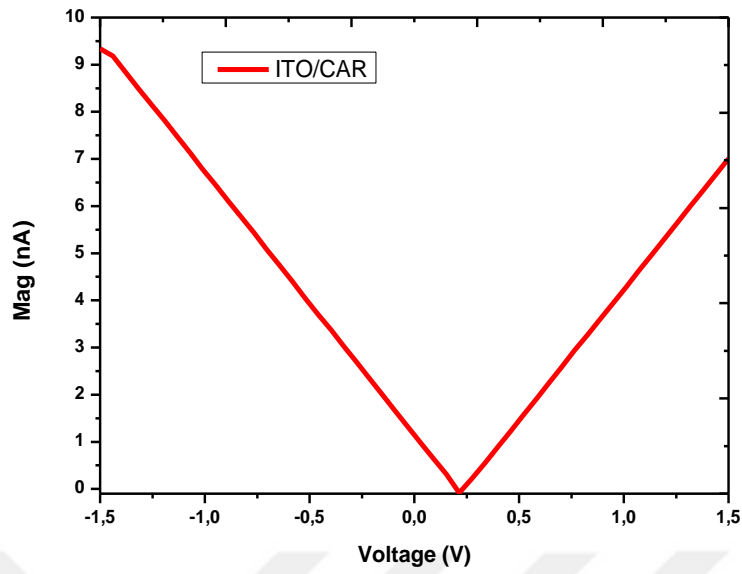


Figure 3.24 : Surface Potential of ITO/CAR

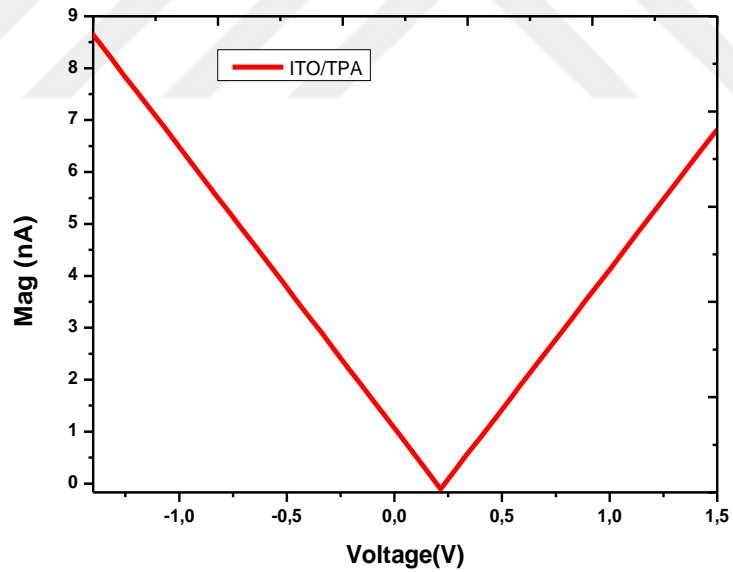


Figure 3.25 : Surface Potential of ITO/TPA

The surface potential of bare ITO, ITO/CAR and ITO/TPA were measured as 0,113 mV, 0,211 mV and 0,216 mV respectively. KPFM results show that, CAR and TPA materials increased the surface potential of ITO. It means that the work function of

ITO/CAR and ITO/TPA surface close to the HOMO level of TPD, which shows it will increase the hole injection from ITO to TPD.

Table 3.8 shows the surface potential values of modified and unmodified ITO.

Table 3.8 : Surface potential of Bare ITO and modified ITO with CAR and TPA

	Bare ITO	ITO/CAR	ITO/TPA
Surface Potential	~ 0,113 mV	~ 0,211 mV	~ 0,216 mV

3.2.3 Contact angle results

As known, ITO has a hydrophilic surface and when a fluid contact with ITO surface, it is spread over a large area of surface. In this study, distilled water was used as fluid. Figure 3.24 shows the contact angle of bare ITO, ITO/CAR and ITO/TPA surface. As seen in this figure, modified ITO has a larger contact angle according to bare ITO. Because, TPA and CAR molecules make a barrier between ITO and fluid.

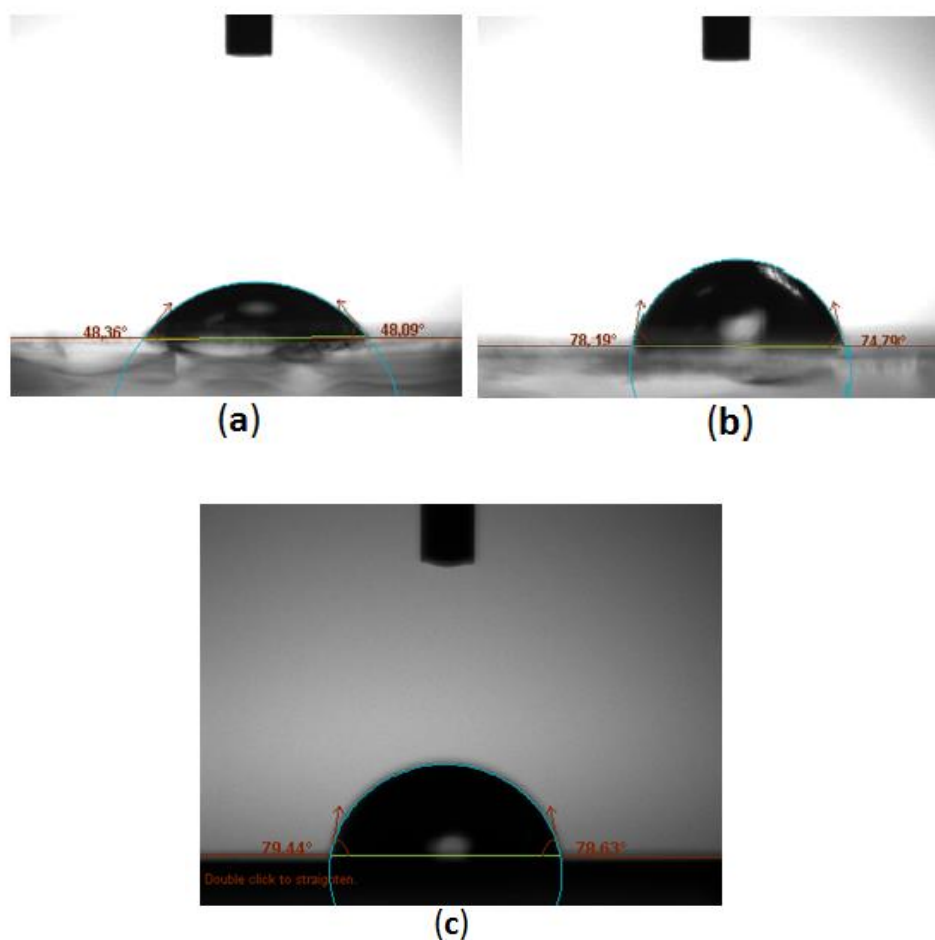


Figure 3.26: Contact angle on Bare ITO (a), ITO/CAR (b) and ITO/TPA (c)

4. CONCLUSIONS

Indium thin oxide (ITO) has been widely used as anode materials in OLED devices because of its high conductivity ($\sim 10^4$ s/cm), high transparency ($\sim 90\%$ at visible range) and high work function (~ 4.7 eV) [36]. In OLED devices, ITO is direct contact with organic layer, but the work function of metal electrode (ITO) and energy level of organic materials have large injection barrier. This barrier lead to poor charge injection and low efficiency[29]. In this thesis, we focused on solving this problem and to solve this problem ITO substrates were modified with SAM materials to increase HOMO energy level of ITO. SAM materials are one of the most promising techniques to modify ITO surface due to its ease of processing and low cost. In this study, TPA and CAR materials were used as SAM materials. After ITO was modified with SAM materials, OLED device performance was increased with respect to the reference devices, which also includes bare ITO.

In Chapter 1, brief information was given about organic light emitting diode, its historical development and its application area. Then the device structure of OLEDs was explained. After the device structure was given, principle of OLEDs operation was explained with charge injection. And then anode materials, cathode materials, hole transport materials, electron transport, and emissive materials were given. In addition, SAM material properties and its techniques were given. Finally, OLEDs efficiency was explained.

In chapter 2 experiment details was given. Firstly, the step of OLED preparation was determined. Then, etching procedure, cleaning procedure and oxygen plasma procedure of ITO substrates was explained. After that surface treatment of ITO with SAM molecules was given. Afterwards, thermal evaporation of organic and metallic layer and also device configuration of OLED devices were explained. Finally, AFM surface characterization, KPFM surface characterization, cyclic Voltammetry characterization, contact angle characterization and electrical and optical characterization were explained.

The experimental results are given in detail in Chapter 4, in this thesis. First, cyclic Voltammetry measurements were performed to determine the HOMO energy level of 'TPA and CAR' SAM molecules. According to CV results TPA and CAR HOMO energy level was determined -5,32 V and -5,58 V, respectively. In addition, energy diagram of devices with TPA and CAR described by means of Figure 3.3. As will be clearly understood from the figure TPA molecules are more suitable than CAR molecules for metallic electrode (ITO) and organic molecules (TPD or NPB). So that modified ITO with TPA devices should show better performance than modified ITO with CAR devices.

After CV results, I-V measurements, luminance, current efficiency, power efficiency and electroluminescence of devices was discussed. In this thesis, ITO/TPD/Alq₃/Al, ITO/CAR/TPD/Alq₃/Al, ITO/CAR/PEDOT:PSS/TPD/Alq₃/Al, ITO /TPA/ TPD/Alq₃/Al and ITO/TPA/PEDOT:PSS/TPD/Alq₃/Al devices were compared to reference devices (ITO/TPD/Alq₃/Al, ITO/PEDOT:PSS/TPD/Alq₃/Al). Turn on voltage of reference devices were 8,0 V and 12,5 V for ITO/PEDOT:PSS and ITO/TPD, respectively. Modified devices (ITO/TPA, ITO/TPA/PEDOT:PSS, ITO/CAR, ITO/CAR/PEDOT:PSS) almost have the same turn on voltage (between 8,0 V – 8,3 V) with ITO/PEDOT:PSS device. Also, they have a low turn on voltage according to turn on voltage of bare ITO (12,5 V). These device luminances, current efficiencies and power efficiencies were given in Table 3.6. As can be seen from the table, all device performances are increased after ITO was modified.

To determine surface characterization of ITO Atomic Force Microscopy, Kelvin Probe Force Microscopy and contact angle methods were used. AFM was used to obtain the surface topography and surface roughness of modified and unmodified ITO. The results show that, unmodified ITO has a higher surface roughness (4,3 nm for bare ITO) than modified ITO with CAR (3,9 nm for ITO/CAR) and TPA (3,4 nm for ITO/TPA). That can be interpreted as TPA and CAR molecules were covered ITO surface and filling the vacancies or holes. That process decreases the roughness of ITO.

In order to determine the surface potential of modified and unmodified ITO substrate KPFM was used. The surface potential of bare ITO, ITO/CAR and ITO/TPA were measured as 0,113 mV, 0,211 mV and 0,216 mV respectively. KPFM results show that, CAR and TPA molecules increased the surface potential of ITO. It means that

the work function of ITO/CAR and ITO/TPA surface close to the HOMO energy level of TPD.

Finally, surface characterization was analyzed with contact angle. As we know ITO has a hydrophilic surface and when a fluid contact with ITO, it is spread over a large area of surface. The contact angle of bare ITO, ITO/CAR and ITO/TPA were obtained as $\sim 48^\circ$, $\sim 78^\circ$ and $\sim 79^\circ$ respectively. After ITO were modified with CAR and TPA molecules contact angle was increased. Because, they make a barrier between ITO and fluid.

To summarize, we modified ITO to increasing the efficiency of organic light emitting diode by using self-assembled monolayers. TPA and CAR molecules were used as SAM materials. According to the cyclic voltammetry results both TPA and CAR molecules increased the work function of ITO. But, TPA is more suitable for ITO and TPD, because it makes an energy level step between the ITO and TPD. So, devices with TPA molecules have better electrical and optical results. However, TPA and CAR SAM molecules effect the electrical and optical device efficiency, which is clearly observed with characterization method.

The OLED devices photo, which is manufactured in this study was given in photographed in Figure 4.1.

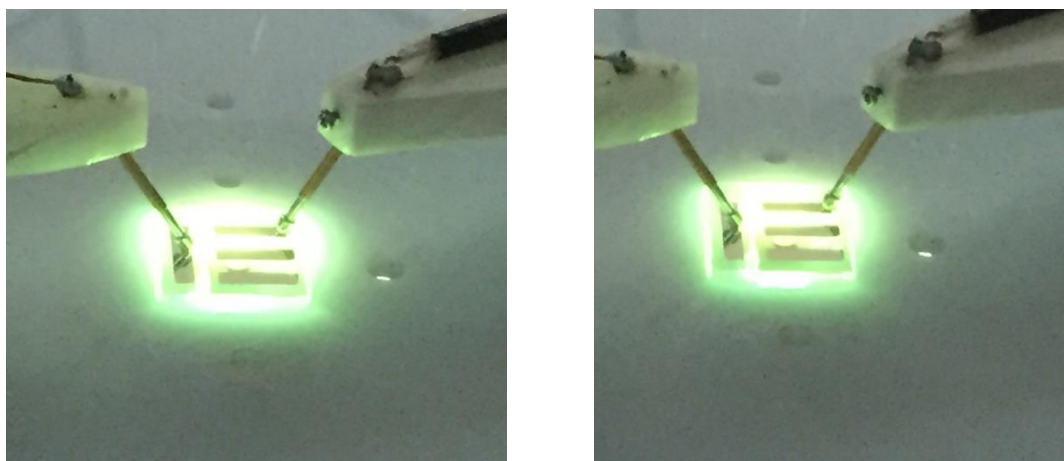


Figure 4.1 : Photos of OLED devices

REFERENCES

1. **Helfrich, W.** and **W. Schneider**, *Recombination radiation in anthracene crystals*. Physical Review Letters, 1965. **14**(7): p. 229.
2. **Tang, C.W.** and **S. VanSlyke**, *Organic electroluminescent diodes*. Applied physics letters, 1987. **51**(12): p. 913-915.
3. **Geffroy, B., P. Le Roy, and C. Prat**, *Organic light-emitting diode (OLED) technology: materials, devices and display technologies*. Polymer International, 2006. **55**(6): p. 572-582.
4. **Karzazi, Y.**, *Organic Light Emitting Diodes: Devices and Applications*. J. Mater. Environ. Sci, 2014. **5**(1): p. 1-12.
5. **Li, Z., Z.R. Li, and H. Meng**, *Organic light-emitting materials and devices*. Vol. 111. 2006: CRC press.
6. **Wang, Z.**, *Design of High Performance Organic Light Emitting Diodes*. 2012, University of Toronto.
7. **Wang, J., et al.**, *High efficiency organic light-emitting diodes with yellow phosphorescent emission based on a novel iridium complex*. Semiconductor science and technology, 2007. **22**(2): p. 25.
8. **Wu, C.**, *New materials and device structure for organic light-emitting diodes*. 2010: University of Southern California.
9. **Wenjin, Z., et al.**, *The effect of the hole injection layer on the performance of single layer organic light-emitting diodes*. Journal of Applied Physics, 2014. **116**(22): p. 224502.
10. **Yu, S.-Y.**, et al., *Effect of ITO surface modification on the oled device lifetime*. Langmuir, 2014. **30**(25): p. 7369-7376.
11. **Pereira, L.F.**, *Organic Light Emitting Diodes: The Use of Rare Earth and Transition Metals*. 2012: CRC Press.
12. **Ganzorig, C., et al.**, *Current-voltage behavior in hole-only single-carrier devices with self-assembling dipole molecules on indium tin oxide anodes*. Applied physics letters, 2006. **89**(26): p. 3501.
13. **Kim, H., et al.**, *Doped ZnO thin films as anode materials for organic light-emitting diodes*. Thin solid films, 2002. **420**: p. 539-543.
14. **Fehse, K., et al.**, *Highly Conductive Polymer Anodes as Replacements for Inorganic Materials in High-Efficiency Organic Light-Emitting Diodes*. Advanced Materials, 2007. **19**(3): p. 441-444.
15. **Marks, T., et al.**, *Progress in high work function TCO OLED anode alternatives and OLED nanopixelation*. Synthetic Metals, 2002. **127**(1): p. 29-35.
16. **Tang, C.W.** and **S.A. VanSlyke**, *Organic electroluminescent diodes*. Applied physics letters, 1987. **51**(12): p. 913-915.
17. **Yamada, T.** and **H. Kaji**, *Planarity of triphenylamine moieties of a typical hole-transport material for OLEDs, N, N'-diphenyl-N, N'-di (m-tolyl)*

- benzidine (TPD), in the amorphous state.* Journal of Molecular Structure, 2009. **927**(1): p. 82-87.
18. **Zhang, S., et al.,** *1-(N-phenylamino) naphthalene oligomers as novel hole transport materials for highly efficient green electrophosphorescence.* Dyes and Pigments, 2015. **118**: p. 1-8.
 19. **Kwak, J., et al.,** *Hole transport materials with high glass transition temperatures for highly stable organic light-emitting diodes.* Thin Solid Films, 2012. **520**(24): p. 7157-7163.
 20. **Zhuang, J., et al.,** *A novel electron transport material with triazole and diphenylphosphine oxide moieties for high efficiency OLEDs.* Tetrahedron, 2013. **69**(43): p. 9038-9044.
 21. **AYDIN, H.,** *INTERFACE PROPERTIES OF MODIFIED INDIUM TIN OXIDE BASED ORGANIC LIGHT EMITTING DIODES WITH FUNCTIONAL AROMATIC MOLECULES.* 2011, İzmir Institute of Technology.
 22. **Kafafi, Z.H.,** *Organic electroluminescence.* 2005: CRC Press.
 23. **Nam, E., et al.,** *Electroluminescence and impedance analyses of organic light emitting diodes using anhydride materials as cathode interfacial layers.* Thin Solid Films, 2009. **517**(14): p. 4131-4134.
 24. **Park, S., C. Lee, and W. Song,** *Enhanced electron injection in organic light-emitting devices using Al/LiF electrodes.* Current Applied Physics, 2001. **1**(1): p. 116-120.
 25. **Sun, Z., et al.,** *Buffer-enhanced electron injection in organic light-emitting devices with copper cathode.* Organic electronics, 2013. **14**(2): p. 511-515.
 26. **Nuzzo, R.G. and D.L. Allara,** *Adsorption of bifunctional organic disulfides on gold surfaces.* Journal of the American Chemical Society, 1983. **105**(13): p. 4481-4483.
 27. **Tokudome, Y., et al.,** *Enhanced hole injection in organic light-emitting diodes by optimized synthesis of self-assembled monolayer.* Organic Electronics, 2011. **12**(10): p. 1600-1605.
 28. **Chong, L.-W., Y.-L. Lee, and T.-C. Wen,** *Surface modification of indium tin oxide anodes by self-assembly monolayers: Effects on interfacial morphology and charge injection in organic light-emitting diodes.* Thin Solid Films, 2007. **515**(5): p. 2833-2841.
 29. **Zhao, Y., et al.,** *Systematic Investigation of Surface Modification by Organosiloxane Self-Assembled on Indium–Tin Oxide for Improved Hole Injection in Organic Light-Emitting Diodes.* ACS applied materials & interfaces, 2014. **6**(6): p. 4570-4577.
 30. **Yildirim, O.,** *Self-assembled monolayers on metal oxides: applications in nanotechnology.* 2010: University of Twente.
 31. **Aswal, D., et al.,** *Self assembled monolayers on silicon for molecular electronics.* Analytica chimica acta, 2006. **568**(1): p. 84-108.
 32. **Adachi, C., et al.,** *Nearly 100% internal phosphorescence efficiency in an organic light-emitting device.* Journal of Applied Physics, 2001. **90**: p. 5048-5051.
 33. **Forrest, S.R., D.D. Bradley, and M.E. Thompson,** *Measuring the Efficiency of Organic Light-Emitting Devices.* Advanced Materials, 2003. **15**(13): p. 1043-1048.

34. **Yu, G. and J. Wang**, *Organic Light-Emitting Devices and Their Applications for Flat-Panel Displays*. 2007, Taylor and Francis Group.–2006.–655.–P. p. 1-45.
35. **Shinar, J. and V. Savvateev**, *Introduction to organic light-emitting devices*. 2004: Springer.
36. **Dong, W.J., et al.**, *Effect of ultraviolet–ozone on ITO/P3HT interface for PEDOT: PSS-free polymer solar cells*. *Solar Energy Materials and Solar Cells*, 2013. **109**: p. 240-245.
37. **Wang, D., et al.**, *Improving Atomic Force Microscopy Imaging by a Direct Inverse Asymmetric PI Hysteresis Model*. *Sensors*, 2015. **15**(2): p. 3409-3425.
38. **Hinterdorfer, P. and Y.F. Dufrêne**, *Detection and localization of single molecular recognition events using atomic force microscopy*. *Nature methods*, 2006. **3**(5): p. 347-355.
39. **Kikukawa, A., S. Hosaka, and R. Imura**, *Silicon pn junction imaging and characterizations using sensitivity enhanced Kelvin probe force microscopy*. *Applied Physics Letters*, 1995. **66**(25): p. 3510-3512.
40. **Nonnenmacher, M., M. o'Boyle, and H. Wickramasinghe**, *Kelvin probe force microscopy*. *Applied physics letters*, 1991. **58**(25): p. 2921-2923.
41. **Kissinger, P.T. and W.R. Heineman**, *Cyclic voltammetry*. *Journal of Chemical Education*, 1983. **60**(9): p. 702.
42. **Yuan, Y. and T.R. Lee**, *Contact angle and wetting properties*, in *Surface science techniques*. 2013, Springer. p. 3-34.
43. **Kwok, D., et al.**, *Contact angle measurements and contact angle interpretation. 1. Contact angle measurements by axisymmetric drop shape analysis and a goniometer sessile drop technique*. *Langmuir*, 1997. **13**(10): p. 2880-2894.
44. **De Jong, M., L. Van Ijzendoorn, and M. De Voigt**, *Stability of the interface between indium-tin-oxide and poly (3, 4-ethylenedioxythiophene)/poly (styrenesulfonate) in polymer light-emitting diodes*. *Applied Physics Letters*, 2000. **77**(14): p. 2255-2257.
45. **Jørgensen, M., K. Norrman, and F.C. Krebs**, *Stability/degradation of polymer solar cells*. *Solar Energy Materials and Solar Cells*, 2008. **92**(7): p. 686-714.

URL1 : <http://www.sciguru.org/newsitem/10944/Researchers-create-worlds-most-efficient-flexible-organic-light-emitting-diodes-plastic>

URL 2 : <http://www.clipartpanda.com/categories/microscope-diagram-and-functions>